7-31-2020

Durable Hydrophobic Polymer Surfaces

Matthew Seitz
ms3897@rit.edu

R·I·T

Durable Hydrophobic Polymer Surfaces

by

Matthew Seitz

A Thesis Submitted in Partial Fulfillment of the Requirements for the

Degree of Master of Science in Materials Science and Engineering

Department of Chemistry and Materials Science

College of Science

Rochester Institute of Technology

Rochester, NY

July 31, 2020

Committee Approval

Dr. Christopher Collison — Date
Thesis Advisor

Dr. Massoud Miri — Date
Committee Member

Dr. Michael Pierce — Date
Committee Member

Dr. Scott Williams — Date
Committee Member

1. Abstract

Highly hydrophobic materials and surfaces are useful for a wide range of applications such as waterproof clothing, self-cleaning windows, reducing drag on watercraft, preventing ice buildup, and designing oil/water separators. However, the hydrophobicity of these materials decreases over time though surface wear, presenting a significant drawback. In this work, we demonstrate a solution to this poor durability through surfaces which are renewed with wear, continually exposing a new hydrophobic surface.

Materials can be made more hydrophobic through the addition of surface texture or microstructure. Typically, as this texture is worn smooth through use and abrasion, the material steadily loses its hydrophobic property. This can be overcome by designing materials with a consistent, textured microstructure through the entire bulk, not only at the surface.

This consistent morphology can be produced from interconnected microparticles. Materials produced in this way can retain a rough surface texture despite wear; as each layer is worn away, a new layer with an identical morphology is exposed and the material remains hydrophobic. The hydrophobicity of this structure is demonstrated both before and after abrasion wear. The hydrophobicity of these surfaces is compared to similar textured surfaces that lack this "renewability."

Contents

2. Introduction

Materials can be described as either being *hydrophilic* or *hydrophobic* based on how that material interacts with water. When a droplet of water falls on a highly hydrophilic surface, the droplet will spread to form a thin film, maximizing the contact area between the droplet and the material surface. Conversely, water falling onto a highly hydrophobic surface will contract into spherical droplets and minimize the contact between the liquid and material. In both cases, the liquid only interacts with the outermost surface of the material, not the bulk of the material. Broadly, a surface can be made more hydrophobic by modifying its structure or morphology,[1,2] or by applying a surface coating[3] like the non-stick coating on a cooking pan. Hydrophobicity is a useful property for a wide range of applications: windows can become self-cleaning,[3] drag on watercraft can be reduced,[3,4] ice buildup on airplanes and powerlines can be prevented,[3,5,6] and oil/water separators can be developed.[7,8] However, many hydrophobic surface treatments and coatings suffer from poor durability.[9,10]

As materials and surfaces are used, the hydrophobic surface texture can be worn smooth or the hydrophobic coating can be worn away. When this occurs, the material will lose its hydrophobicity. One approach to overcoming this poor durability is to design materials with a "renewable" surface structure. If materials can be designed to have a consistent morphology through the bulk of the material, then as the top layer of the material is worn away a similar morphology would be exposed, maintaining the material's hydrophobicity.

Surfaces or materials with this combination of hydrophobic texture and consistent morphology could be produced by sintering microparticles together to form a cohesive surface. Sintering is a process where discrete particles are compacted, typically through heat and/or pressure, to form a single solid.[11–13] This process typically results in the destruction of microstructures as molecular diffusion between adjacent particles produces a uniform, smooth surface. However, by controlling the extent of this sintering, this diffusion can be used to form strong interconnections between particles while still maintaining a "packed spheres" morphology through the bulk of the material.

Two methods of achieving this "packed spheres" morphology are explored. The first method is based on the work of Hoogenboom, *et al.*[14] who demonstrated that, through heating and cooling, a polystyrene-polymethyl methacrylate (PS-PMMA) copolymer could be dissolved and precipitated to form polymer microspheres. These precipitated particles then settled and self-assembled into a cohesive surface. While Hoogenboom, *et al*. only explored the change in polymer solubility with temperature, I hypothesized that these self-assembled structures could also be used as a durable, abradable, hydrophobic surface. Achieving and demonstrating this improved hydrophobicity required careful tuning of the solvent blend,

polymer concentration and molecular weight, heating and cooling rates, as well as the development of a testing apparatus and procedures, which culminated in the development of a thermally induced phase separation (TIPS) process compatible with PMMA.

While this process is effective in both producing polymer microparticles and assembling them into a durable surface, it does face several significant disadvantages. The TIPS process has been shown to be effective with PMMA, but not with other polymers. If this process could be modified to work with other, more durable or chemically resistant polymers, these surfaces could be viable for a wider range of applications. Modifying this TIPS process requires finding a new solvent system, compatible with new polymers. While this TIPS process will yield a certain distribution of particle sizes with PMMA and one solvent blend, different conditions will be necessary for other polymers. Hansen Solubility Parameters (HSP) theory[15,16] could be used to predict and develop new solvent blends which would enable the TIPS process to be compatible with new polymers.

A second method explored to produce these surfaces breaks the one-pot TIPS process into discrete steps. An emulsion-based process can be used to produce microspheres from a wide variety of polymers,[17,18] greatly improving the applicability of these surfaces. After these microspheres are produced, they can be isolated and sintered to form surfaces with a TIPS-like morphology. By separating the process into its individual steps, each step can be more effectively controlled and the hydrophobicity of the final surface can be optimized.

Both of these methods produce surfaces and materials with randomly arranged particles, yielding non-ordered surface roughness. The hydrophobicity of these materials are compared against ordered patterns produced through photolithographic processes. By using photolithography, carefully tuned patterns or arrays of pillars can be produced with a high degree of control over their exact size, shape, and spacing.[19] These patterns are initially etched into silicon wafers, then replicated with PDMS to produce an inverted copy.[20] The hydrophobicity of these replicas can then be compared to surfaces produced by other methods.

3. Theory

3a. Wettability and Hydrophobicity

Wettability describes how a liquid interacts with a solid surface.[21] A liquid's surface tension (*cohesive* intermolecular forces) pulls the liquid into a tight ball, minimizing the droplet's surface area while *adhesive* forces between the solid surface and the liquid cause spreading, increasing the contact area between the two materials. If the solid-liquid adhesive forces are much stronger than the liquid-liquid cohesive forces, the liquid will spread to form a thin film over the surface (complete wetting). Conversely, if cohesive forces greatly exceed adhesive forces, the liquid will contract into discrete droplets, minimizing their contact with the surface (partial wetting)[22]. Contact angle is the typical metric used to describe the equilibrium between these two sets of forces and represents the angle formed where the liquid-gas interface of a droplet meets a solid surface (Figure 1, below).

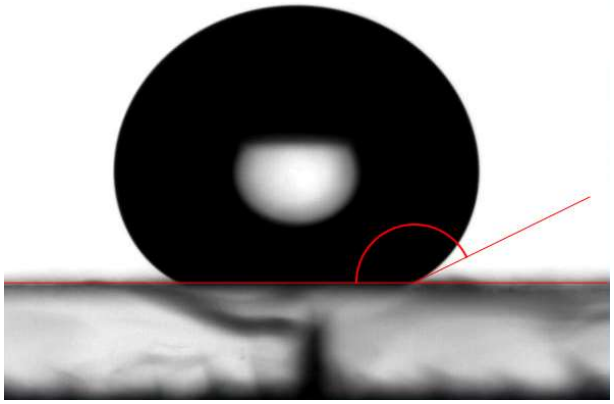

Figure 1 – Large contact angle (red) between a water droplet and a superhydrophobic PVC surface (153°)

This contact angle varies both from material to material and from liquid to liquid. When water is used as the test droplet at the surface of the solid, materials can be described as *hydrophilic* if the contact angle is below 90°, or as *hydrophobic* if the contact angle is greater than 90°. Materials with a contact angle greater than 150° are termed *superhydrophobic*.

For smooth, flat surfaces, contact angles can be predicted using Young's equation[23]:

$$\cos\theta_{Young} = \frac{\gamma_{sv} - \gamma_{sl}}{\gamma_{lv}}$$

Where γ represents surface tension, and *s, l,* and *v* represent solid, liquid, and vapor states. However, because this effect is completely dependent on surface interactions, surface roughness/inhomogeneity can have a major impact on observed contact angles and wettability properties. This rough surface behavior can be separated into two regimes – in the Wenzel state, the liquid droplet fills the small voids and

crevices on the irregular surface, while in the Cassie-Baxter state, the liquid does not fill the voids and is supported by small pockets of air as well as the surface itself (Figure 2, below).

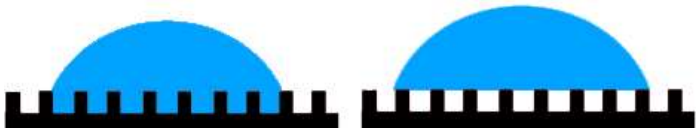

Figure 2 - Droplet in a Wenzel State (left) and in a Cassie-Baxter State (right)

These two states lead to significantly different contact angles, due to differences in contact area between the solid and liquid. In the Cassie-Baxter state[1], the droplet is only in direct contact with a fraction of the total surface area, leading to reduced total solid-liquid adhesive forces and an increased contact angle. However, in the Wenzel state[2], the contact area between the droplet and the surface increases as the liquid fills voids/pores and contacts the "walls" of the voids as well as the surface. This leads to more complex wetting behavior, depending on the relative strengths of the liquid surface tension and solid surface energy.

In all liquids, cohesive forces between molecules within the bulk are balanced, while these same forces are unbalanced at the air-material interface, as shown in Figure 3, below. For liquids, these unbalanced forces lead to a net force inward, toward the bulk of the material and an overall contraction to minimize surface area. The liquid's surface tension quantifies this net force.

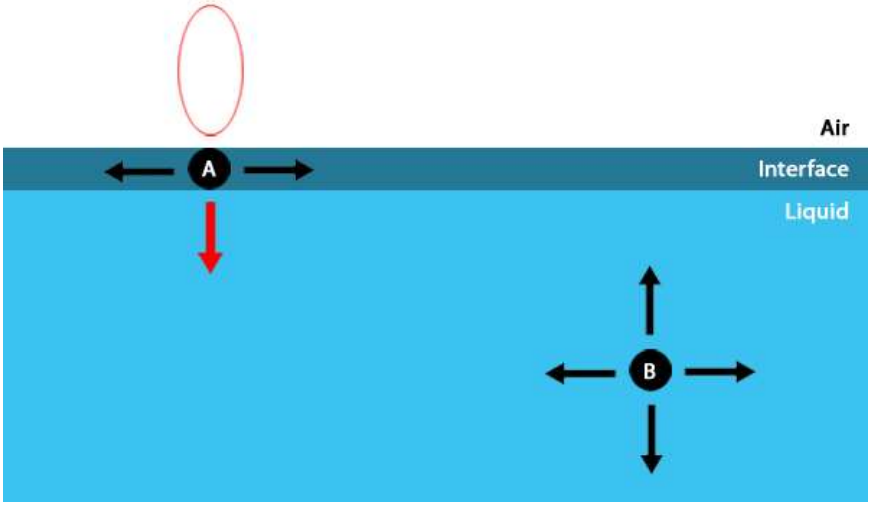

Figure 3 - (A) Unbalanced cohesive forces at liquid-air interfaces and (B) balanced cohesive forces within the bulk of the material

With solids, similar unbalanced intermolecular bonds at interfaces cause surface molecules to have excess energy when compared to identical molecules within the bulk. This causes the surface to be less energetically favorable than the bulk of the material. Just as liquids have surface tension, solids have

surface free energy, or simply surface energy. This excess free energy leads to attractive forces between the solid surface and other materials in contact with the surface, like liquid droplets.

In the case of inherently hydrophilic (flat) materials, high surface energy overpowers water's surface tension and droplets spread. If this same material surface is then made rough, a droplet in the Wenzel state would be pulled into the new surface voids, increasing the solid-liquid contact area, and amplifying the difference between the strong surface energy and weaker liquid surface tension. This larger total energy difference increases the spreading behavior of the droplet, resulting in an overall lower contact angle and larger droplet footprint. Conversely, an inherently hydrophobic (flat) material's lower surface energy is overwhelmed by water's high surface tension, allowing the droplet to form a tight ball, minimizing its contact area. If this material surface is subsequently made rough and voids are filled by a droplet in the Wenzel state, adhesive and cohesive forces find equilibrium with a smaller droplet footprint, leading to a higher contact angle.

The contact angle for droplets in the Wenzel state can be predicted with the Wenzel Equation[2], a modification of Young's Equation:

$$\cos\Theta_W = R\cos\Theta_{Young}$$

The predicted contact angle, Θ_W, is dependent on both the material's inherent contact angle (Θ_{Young}), and a roughness factor, *R*, defined as the ratio of true solid surface area to the planar or projected surface area, describing the degree of surface roughness present. The predicted contact angle for droplets in the Cassie-Baxter state is calculated from two components. One fraction of the droplet is supported by the solid surface (*f*), while the remaining fraction (*1-f*) is supported by air[1]:

$$\cos\Theta_{C-B} = f\cos\Theta_1 + (1-f)\cos\Theta_2$$

The contact angle between the water droplet and flat surface can be predicted with Young's Equation (Θ_{Young}). Water forms a contact angle of 180° with air (Θ_2), allowing us to substitute $\cos 180° = -1$ and simplify the Cassie-Baxter Equation to:

$$\cos\Theta_{C-B} = f\cos\Theta_{Young's} - (1-f)$$

One shortcoming of these models/equations is a lack of consideration of feature size. Intuitively, as gaps between adjacent features increase in size, a droplet would be increasingly unlikely to bridge the gap between features (filling those voids in a Wenzel state). However, both the Wenzel roughness factor and Cassie-Baxter surface fraction are unitless ratios with no distinction between (for example) nano-scale features and macro-scale features. This led me to hypothesize that a critical feature size/spacing exists

which delineates these two wetting states. Features smaller than this critical size would lead to Cassie-Baxter state droplets, while larger features would lead to a Wenzel state.

3b. Manufacturing Hydrophobic Surfaces

Current methods used to manufacture (super)hydrophobic surfaces are widely varied, but fall into three general categories – introduction of surface roughness, addition of a hydrophobic coating, or a combination of both[24,25]. However, the vast majority of these methods suffer from one critical drawback – low durability of these improved hydrophobic properties[9,10].

As shown by the work of Wenzel[2], increasing the surface roughness of a hydrophobic material can further improve its hydrophobic properties, resulting in an increased contact angle. Cassie and Baxter[1] also showed that, through the addition of carefully designed surface roughness, normally hydrophilic materials can be made to be hydrophobic. Researchers have used numerous methods to apply this roughness to a range of materials. These methods can be (again) divided into two general categories, periodic patterns and non-ordered methods.

Some non-ordered methods include chemical or plasma etching, solution immersion, laser ablation, electrodeposition and electrospinning, spray coating, and phase separation deposition methods.[24,25] These approaches involve removing (through etching, immersion, ablation) or adding (through electrodeposition/spinning, spray coating, phase separation deposition) material, forming randomly arranged micro/nanoscale hills and voids which provide the necessary surface roughness to increase the surface hydrophobicity. By adjusting experimental parameters (plasma current, etchant concentration, laser power, exposure time, etc.), feature size distribution and feature density can be modified/controlled, allowing for tuning/optimization of the degree of roughness and hydrophobicity. Conversely, periodic methods can be used to produce carefully tuned, repeating arrays of uniform pillars/pyramids. This is most commonly achieved through photolithography or electron beam lithography. These approaches offer much finer control over the shape, size, spacing, and overall morphology of the final shapes/features used in the hydrophobic surface[19].

Surfaces can also be made hydrophobic through the application of a uniform (smooth) coating of low surface energy material, typically a silane or fluoropolymer[26]. This approach takes advantage of the fact that hydrophobicity is purely a surface effect – the inner/bulk material does not affect the surface's hydrophobic properties. Through this method, bulk properties (electrical/thermal conductivity, magnetic response, overall robustness, etc.) are only minimally affected (if at all), while hydrophobic properties can be dramatically improved. This approach can be combined with many of the previous methods for increasing surface roughness (above) to produce highly effective superhydrophobic surfaces. This

secondary treatment is sometimes necessary, as simply increasing surface roughness can lead to droplets in a Wenzel state and a decrease in contact angle/surface hydrophobicity[24,25].

One problem shared by the vast majority of these surface manufacturing approaches is the durability of the surface roughness/coating/hydrophobic state. The necessary micro/nanoscale surface roughness which improves the surface's hydrophobicity, or thin/monolayer coatings can quickly be abraded flat, rendering them ineffective[9,10]. The majority of methods currently used to produce these hydrophobic surfaces only produce one layer of roughness but once that outermost layer is worn away, only the flat, non-textured, bulk material remains. Lithographic processes address this problem through the use of arrays of pillars – extending the effective lifespan of the surface by producing taller features. However, these pillars are not a complete solution; as pillars become taller, they also become more sensitive to deforming/breaking under shear stresses.

One possible solution to the lack of hydrophobic surface durability could arise from phase separation processes. Hoogenboom, *et al.*[14] demonstrated that PS-PMMA could be dissolved, reprecipitated and allowed to settle and self-assemble into a cohesive surface. I hypothesized that this microparticle self-assembly could not only yield an effective, rough, hydrophobic surface, but also could produce a surface with much more durable hydrophobic properties. Rather than only consisting of a single rough and textured layer, as in most typical manufacturing methods, these surfaces would consistently "renew" as the bulk was abraded; as each layer is worn away, a new, identical layer would be revealed.

3c. Tuned Hydrophobic Patterns Through Photolithography

In contrast to chemical processes, which produce randomly distributed surface roughness, lithographic processes allow for submicron control over the exact size, shape, spacing, and overall design of surface features[27]. These processes offer a tremendous opportunity to systematically vary aspects of the hydrophobic pattern and optimize its design. By varying the shape and spacing of engineered surface structures/features, the Wenzel roughness factor (R) and Cassie-Baxter contact fraction (f) can be closely controlled. After the Young's contact angle is measured for a given smooth material surface, the Wenzel and Cassie-Baxter contact angles for textured surfaces constructed from the same material can be predicted. These predicted contact angles can then be compared to contact angle measurements made with manufactured surfaces to determine which patterns lead to droplets in a Wenzel state and which patterns lead to droplets in a Cassie-Baxter state. I hypothesize that a critical feature size will be found which will delineate these two states (Wenzel vs Cassie-Baxter states). Patterns using features below this critical size will result in droplets in a Cassie-Baxter state, while patterns using features larger than this critical size will result in droplets in a Wenzel state.

These types of lithographic patterns are typically produced on silicon wafers. Manufacturing these patterns first requires coating the wafer with a light-sensitive photoresist. The physical structure of this photoresist changes upon exposure to light – forming (negative photoresist) or breaking (positive photoresist) chemical crosslinks. This (localized) change in crosslinking density changes the polymer solubility properties – an effective solvent for the non-crosslinked polymer is ineffective for the crosslinked polymer. Control over what areas are exposed to light is accomplished by either using an opaque mask, or a highly focused laser. After exposure, the photoresist is "developed" and the non-crosslinked regions are dissolved away, exposing bare silicon in the desired pattern[27]. This bare silicon is susceptible to plasma etching – allowing for selective removal of only the "developed" regions of the pattern. By carefully controlling the duration of plasma exposure, the resulting depth of etching can be controlled. However, as the plasma etches and removes exposed silicon, material is removed both from the bottom and the sidewalls of the features, leading to an (undesired) undercut. This can be minimized or eliminated by including passivation steps in the process.[28] Once etching is complete, remaining photoresist can be thermally removed.[29]

In order to prevent damage from this silicon master, replications of this master are often created to produce testing samples.[20] In this process, liquid polydimethylsiloxane (PDMS) is poured over the patterned silicon wafer master, allowed to cure, then carefully peeled from the master revealing an inverted replica of the master's surface pattern. To ensure accurate replication, a degassing step is often used – this removes any air bubbles trapped between the silicon surface and PDMS and ensures full wetting (Wenzel state) of the silicon master. One likely outcome of repetitive replication is that, as pattern features shrink in size and their aspect ratios increase, the PDMS structures could become stuck in the master wafer and tear away from the PDMS bulk, causing imperfections in the replication and damaging the master. To prevent this, a fluorinated silane coating was applied to the silicon wafer prior to PDMS replication as a mold release.[30]

3d. Thermally Induced Phase Separation (TIPS)

While photolithographic processes offer unparalleled control over the precise layout and size of patterns, these processes are not suited to apply a hydrophobic texture to objects larger than few-inch diameter silicon wafers. Photolithography is an excellent approach to produce test samples, but the high cost, complexity, and time needed limits the practicality of this approach. With the goal of developing a process which is more cost effective and can be applied to items of all sizes, other approaches were also tested. Work done by Hoogenboom, *et al*.[14] showed that PS-PMMA copolymers can be dissolved by a heated solution of ethanol and water, despite being completely insoluble at room temperature. Additionally, when this solution is cooled, the copolymer precipitates to form nanosphere micelles which self-assemble and agglomerate.[14] The objective of Hoogenboom's work was to observe and better

understand the effects of temperature on the solubility of this copolymer, with the goal of finding an alternative, non-toxic, green solvent. However, I observed that images of these self-assembled particles appeared to possess an appropriate degree of surface roughness to improve the polymer's hydrophobic behavior. This observation inspired my work, and I hypothesized that this precipitation and self-assembly process could be used to develop novel, durable, hydrophobic surfaces.

In this thermally induced phase separation (TIPS) process, PMMA is initially insoluble in the ethanol/water solvent mixture. As this solution is heated, intermolecular bonds holding the polymer chains together weaken, allowing the polymer chains to disentangle. Over time, this disentanglement leads to the complete dissolution of the polymer and the formation of a single homogenous liquid solution phase. When this solution is cooled, the reverse occurs – polymer chains lose kinetic energy, nucleate, and form nano/microparticles. These particles are initially suspended in a colloid but settle to the bottom of the container through sedimentation as they grow in size.

Particle precipitation and growth occurs as polymer solubility falls. This precipitation is "typically" accomplished through the addition of a non-solvent.[31] As the concentration of the new, poor solvent increases, the dissolved polymer precipitates from solution and forms particles. Keßler *et al*.[31] have found that the rate of addition of this poor solvent determines the final precipitated particle size. The authors describe the addition of poor solvent as a "rate of solvent change"[31] and found that a rapid change (i.e. quickly adding poor solvent) resulted in small particles forming, while a more gradual change resulted in larger particles forming. In this TIPS process, a similar "solvent change" is accomplished instead by cooling the solution. This gradual change in temperature similarly reduces the "quality" of the solvent, leading to precipitation and particle growth.

As the particles increase in size, they reach a critical size where their mass overpowers liquid buoyant forces and the particles will sedimentate and form a layer on the bottom of their container. In this layer, individual particles are in contact with other particles, which allows for polymer chains in adjacent particles to become intertwined. This forms "bridges" between particles and transforms the collection of discrete, separate particles into an interconnected 3D network. These bridges provide strength to the network, while still maintaining surface roughness. This surface roughness makes the surface hydrophobic. Additionally, this interconnected particle morphology will remain consistent throughout the bulk of the material. I hypothesize that this will enable these TIPS surfaces to demonstrate a high degree of durability; as the surface is abraded/worn away, new layers with an identical structure will be exposed, leading to continued hydrophobic behavior.

3e. Hansen Solubility Parameters

One other significant research goal was to replicate the success of the TIPS process with additional (more heat and chemically resistant) polymers to improve the versatility and applicability of the functional material. This required both the selection of new polymers of interest as well as corresponding solvent blends. Solvents and blends were selected using Hansen Solubility Parameters (HSP) theory. Hansen Solubility Parameter (HSP) theory uses four components to describe solvent-polymer interactions. *Solvents* are assigned values (in units of $MPa^{1/2}$) describing the strength of their intrinsic intermolecular bonding forces. The three values are categorized as Dispersion Forces (δD_1), Dipole Interactions (δP_1), and Hydrogen Bonding (δH_1) forces. *Polymers* receive their own three values, one for each of the bonding forces (δD_2, δP_2, and δH_2), with a fourth Interaction Radius (R_a). A solvent-polymer distance (R) is calculated as a sum of square differences between each respective intermolecular bonding force:

$$R = \sqrt{4(\delta D_1 - \delta D_2)^2 + (\delta P_1 - \delta P_2)^2 + (\delta H_1 - \delta H_2)^2}$$

This calculated R distance can then be compared to the polymer's interaction radius; if $R < R_a$, the polymer is predicted to be soluble in the solvent or solvent blend, and if $R > R_a$, the polymer is predicted to be insoluble. This process can be best visualized using a 3D graph, with each of the three bonding forces assigned to a Cartesian axis. In this 3D "HSP space," polymers are represented as spheres, while solvents are represented as points. Solvents which lie within a polymer sphere represent ***good*** solvents, while solvents lying outside the polymer sphere represent ***non***-solvents. When solvents are combined, the blend's Hansen Solubility Parameter values become the weighted average (by volume ratio) of the HSP values of the components, which allows for new solvent blends to take on values that lie inside or at the periphery of the polymer sphere, as desired.

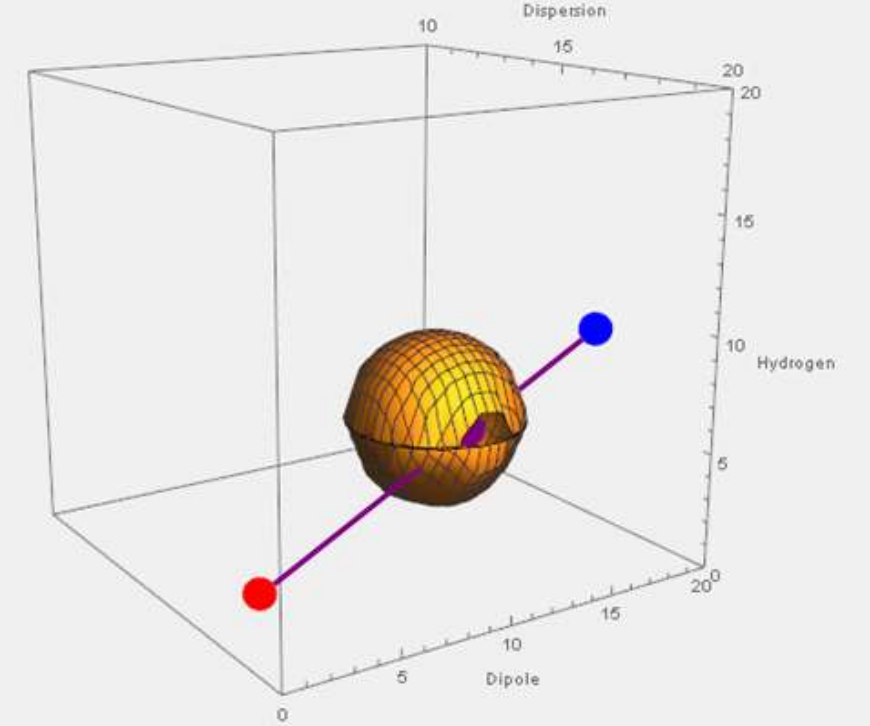

Figure 4 – Ultem (yellow sphere), toluene (red point), and DMSO (blue point) in "HSP space." By mixing these two solvents, the resulting solvent blend can have any set of values on the purple line.

As shown in Figure 4, above, dimethylsulfoxide (DMSO, shown as a blue point) and toluene (shown as a red point) both lie outside the yellow sphere representing the solubility of Ultem (a commercial poly(ether imide), selected for our experiments due to its robustness and high thermal and chemical stability). This (correctly) predicts that neither solvent by itself is a good solvent for Ultem. By mixing these two solvents in varying proportions, this solvent blend can take any value on the line between them (shown as the purple line in Figure 4). By selecting an appropriate ratio of these two non-solvents, a good solvent *blend* can be created (as described by Table 1).

Table 1 – Example HSP values and solubility results

Polymer	**dD**	**dP**	**dH**	**R_a**	
Ultem	18.0	9.2	7.5	3.5	
Solvents	**dD**	**dP**	**dH**	**R – Ultem**	**Result**
DMSO	18.4	16.4	10.2	7.7	Insoluble
Toluene	18.0	1.4	2.0	9.5	Insoluble
4:6 DMSO/Toluene	18.2	10.4	6.9	1.4	Soluble

Temperature effects can also be modeled through HSP, using the solvent's Thermal Expansion Coefficient (α). Dr. Hansen predicts that solvent HSP values decrease as temperature (T) increases above 25°C while polymer HSP values remain constant[16]:

$$\frac{d\delta_D}{dT} = -1.25\alpha\delta_D$$

$$\frac{d\delta_P}{dT} = -0.5\alpha\delta_P$$

$$\frac{d\delta_H}{dT} = -\delta_H(1.22\text{x}10^{-3} + 0.5\alpha)$$

Overall, as temperature increases, solvents move towards the origin in HSP space. Given this model, solvents were selected such that the HSP values of the solvent blend were greater than those of the polymer with the solvent blend HSP coordinates lying outside the polymer sphere at room temperature. However, when this solution is heated, the solvent blend HSP values decrease, reducing the solvent-polymer distance, thus solubilizing the polymer. Once the polymer is fully dissolved, the solution is cooled, ideally inducing re-precipitation into small particles which then settle and form a sedimented surface.

The approach presents several challenges. While HSP values for many solvents are readily available (often directly from Dr. Hansen's work),[15,16] values for polymers are more difficult to find in literature. Furthermore, radius values for these polymers are even less reported and can vary from report to report. These challenges culminate in a wide range of HSP values and radii reported in the literature, as shown by Table 2, below.

Table 2 - Reported HSP Values for PMMA

	Janting[32]	Ferndndez-Pierola[33]	Li[34]
δD	18.7	16.2	18.64
δP	8.6	8.3	10.52
δH	8.9	7	7.51
R_a	6.7	Not Reported	8.59

As a final challenge, some solvents, like chloroform, act as a much more effective solvent than their HSP values would otherwise suggest[16]. For example, chloroform is a good solvent for Ultem, despite a very large radial distance between the two.[35]

3f. Single Emulsion/Solvent Evaporation

As an alternative to using Hansen Solubility Parameters to directly replicate the "one-pot" TIPS process, we also explored processes to first produce microparticles, which could then be separately sintered into a cohesive surface. The most promising and replicable method to produce microparticles is the Single Emulsion/Solvent Evaporation method[17]. In this process, polymer (dissolved in an organic solvent) is added to water. When these immiscible liquids are stirred, they form an emulsion as shear forces break the polymer/solvent phase into droplets within the water phase. The addition of an emulsifier or surfactant, such as poly(vinyl alcohol) (PVA), can help to stabilize this emulsion. These surfactant molecules disperse across the interface between the two immiscible liquids, forming a protective shell[36] as shown in Figure 5, below. This shell acts as a barrier, helping to prevent emulsified droplets from recombining and increasing in size. As the emulsion continues to stir, the emulsified solvent evaporates and the droplets solidify to form microparticles. Any residual PVA left on the surface of these microparticles can then be washed away using water when the microparticles are collected via filtration.

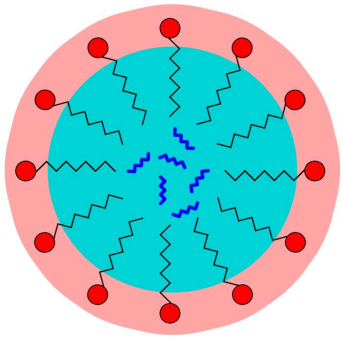

Figure 5 - Simplified cartoon diagram of an emulsion micelle. Surfactant molecules (red with a black tail) arrange on the surface of the micelle, encapsulating the dissolved polymer (blue lines) and separating it from the water phase outside.

Several factors which affect the final micelle size were identified by Sharma, *et al*.[18] Micelle sizes were found to decrease when the emulsion stirring speed was increased or when the dissolved polymer concentration was decreased. As stirring speed increases, the energy added into the system leads to dispersion of the dissolved polymer within the continuous water phase and the formation of progressively smaller micelles. Conversely, when the dissolved polymer concentration increases, the viscosity of the polymer/solvent phase increases. This results in an increase in cohesive forces which resist the stirring-induced dispersion and lead to the formation of larger micelles.[18] I hypothesize that these two parameters can be varied in order to control the size of the microparticles produced through this emulsion process.

Once these micelles have formed, they must be solidified before they can be collected and used to construct hydrophobic surfaces. One process to accomplish this was studied by Rosca, *et al*.[17] Over time, the volatile organic solvent used to dissolve the polymer evaporates away. This causes the dissolved polymer chains to precipitate from solution, entangle, and form the final microparticles. These, now solidified, particles can then be collected through simple vacuum filtration. Once isolated, these polymer microparticles must be formed into a cohesive surface. Unlike the TIPS process, this requires a separate sintering process, described below.

3g. Solvent Sintering

During traditional sintering processes, discrete particles are compacted through a combination of heat and pressure to form a solid with uniform density, without fully melting.[11] This allows easily-processed powders to be formed into strong, durable parts. This process of compaction progresses through several stages, as shown in Figure 5, below. Discrete particles (Figure 6a) initially come into contact with neighboring particles (Figure 6b) through thermal swelling, external pressure, sedimentation, or other processes. Atoms or molecules then begin to diffuse across particle/grain boundaries, forming physical

interconnections between adjacent particles. As sintering progresses, these interconnections steadily increase in size (Figure 6b, 6c, and 6d). If left to progress to completion, sintering fully destroys any microstructure or surface texture and the initial, once discrete, particles become a uniform, homogenous solid[37] (Figure 6d).

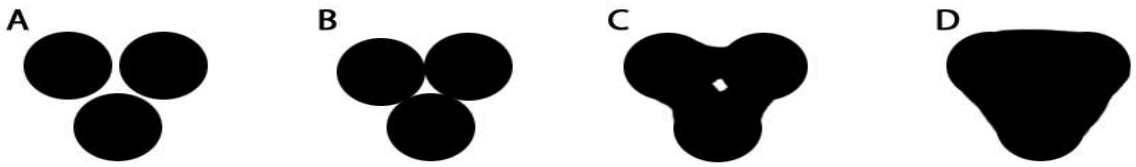

Figure 6(a-d) – Sintering of discrete particles to form a fully compacted solid.

While useful in a variety of applications, the complete elimination of pores/voids is detrimental to the production of rough, hydrophobic surfaces. However, this process could be ceased "early" to yield durable solids which still retain some degree of porosity and surface roughness.

As an alternative to heat and pressure, a solvent/non-solvent solution can be used to sinter polymer particles. This solvent/non-solvent sintering process is accomplished by immersing the polymer microparticles in a sintering solution containing a more-volatile good solvent and a less-volatile non-solvent. This solution begins to dissolve the microparticles, disentangling and unravelling polymer chains near the particle surface[13,36]. As these polymer chains gain more freedom of movement, they become intertwined with chains attached to neighboring particles and form interconnections/bridges between the two without significantly deforming the particles.[12,38] This allows for the formation of a large, interconnected, three-dimensional network of particles while retaining a rough, potentially hydrophobic texture. This process of partial dissolution and interconnection formation is ceased by the evaporation of the good solvent. As this component of the sintering solution is removed, the disentangled polymer chains become locked in place by the increasing proportion of non-solvent which gradually forces polymer chains to re-entangle and solidify.[12,36,38] Since the solvent/non-solvent blend can penetrate through the interstices of the packed powder, I hypothesize that a 3D structure of interconnected spheres will be developed. This would allow the same hydrophobic texture to be maintained as successive layers of particles are worn away through abrasion.

This solvent sintering process has been applied to a range of polymers in the literature for a variety of (primarily bio-medical) applications.[12] While sources from literature do not test the hydrophobicity of solids produced in this manner, they appear to have a TIPS-like morphology. I hypothesize that, through careful control over the extent of sintering, this solvent-based sintering process can be used to produce robust hydrophobic surfaces from polymer microparticles. By controlling the extent of the sintering

process, a “sweet spot” between hydrophobic roughness and large, robust particle interconnections could be found.

3h. Durability of Hydrophobic Surfaces and Patterns

Hydrophobic and superhydrophobic surfaces and materials have been produced from a range of materials and from a range of techniques.[3–8,19,20,24–26,39–41] However, while careful study of the resulting contact angle has been reported, the durability of these surfaces typically goes unreported.[9] Additionally, when surfaces or materials are claimed to be “durable,” each author must develop their own in-house methodology to test for and demonstrate this durability as no generally accepted, standardized method or procedure exists.[9,42,43] This leads to the development of numerous different systems to measure and quantify surface performance and the generation of data which cannot be accurately compared between research groups. These various methods can be challenging to accurately replicate – imprecise and non-replicable testing methods such as abrasion by hand with either sandpaper[39] or cotton swabs[44] are reported by some groups. Attempting to compare results is further complicated by groups reporting the effects of wear or abrasion through changes in different metrics, such as water sliding angle,[44] coefficient of friction,[45] or static contact angle.[39]In this work, care was taken to develop a testing methodology which would be consistent both run-to-run and group-to-group. This process, described fully in Section 5b, below, uses a fixed mass and an electric motor to pull sandpaper across each sample to simulate real-world abrasion wear on the surfaces. Static contact angle measurements can then be taken of surfaces after varying numbers of abrasion cycles to evaluate and compare surface performance over time.

4. Experimental

Our experiments with different methods to manufacture hydrophobic surfaces began by replicating several approaches already published in the literature[40,41] (Sections 4b and 4c). The effect of feature size and spacing on surface hydrophobicity was studied by producing highly tuned patterns through photolithography (Section 4d). The replication of experiments from literature culminated in the discovery of the TIPS process (Section 4e). Finally, work towards adapting the TIPS process to be compatible with new polymers led to the development of surfaces produced from sintered microparticles (Sections 4f and 4g).

4a. Baseline Samples and Measurements

Before the effects of surface patterns on hydrophobicity can be measured, baseline values must be measured. Contact angle measurements were taken on flat, un-textured samples of poly(methyl methacrylate) (PMMA), polystyrene (PS), Ultem (a commercial poly(ether imide)), and polydimethylsiloxane (PDMS). With the exception of PDMS, the polymers were dissolved in organic solvent and spin cast to produce flat surface samples. Samples of PMMA (Polysciences, Inc, Catalog Number 17913, Mw = 100kg/mol) and Ultem (3DXTech, Ultem 1010 3D Printing Filament) were produced by first dissolving the polymer in chloroform (Macron, VWR Catalog Number CAMK444004) at a concentration of 0.1g/mL followed by spin casting at 1000 RPM for 10s. Similarly, PS (Aldrich Chemical Company, Inc, Catalog Number 18242-7, Mw = 250kg/mol) was added to toluene (Macron, VWR Catalog Number MK860816) at a concentration of 0.3g/mL and spin cast at 3000 RPM for 60s. Finally, PDMS (Sylgard-184, Dow Corning) was mixed in a 10:1 ratio, per the included instructions, drop cast onto a silicon wafer, and allowed to cure at room temperature for 72 hours prior to demolding from the silicon wafer.

4b. PVC Phase Separation

Our first attempt to manufacture hydrophobic polymer surfaces utilized phase separation during evaporation to produce a rough, textured surface structure. Following Chen *et al*.'s approach,[40] 0.01g/mL poly(vinyl chloride) (PVC, Sigma-Aldrich, Catalog Number 189588, Mw = 62kg/mol) was dissolved in tetrahydrofuran (THF, TCI, Product Number T2394) at room temperature. Once fully dissolved, an equal volume of 100% ethanol (Deacon Labs, Product Number 2716GEA) was added as a non-solvent. Upon the addition of the non-solvent, the clear solution became slightly opaque with a small amount of precipitate. The solution was briefly mixed on a vortexer (VWR, Mini Vortexer MV1), then set aside to allow any precipitated PVC to re-dissolve into the solution. (Controlled precipitation of polymer materials have been studied for many years, and the idea has been exploited in prior work by Collison[46]). 400µL of this solvent/non-solvent solution was then dispensed via pipettor onto a glass microscope slide

substrate (25mm x 25mm) and allowed to evaporate in a fume hood. After evaporation of the solvent and non-solvent, a slightly rough, white, superhydrophobic surface was left on the glass substrate (Figure 7).

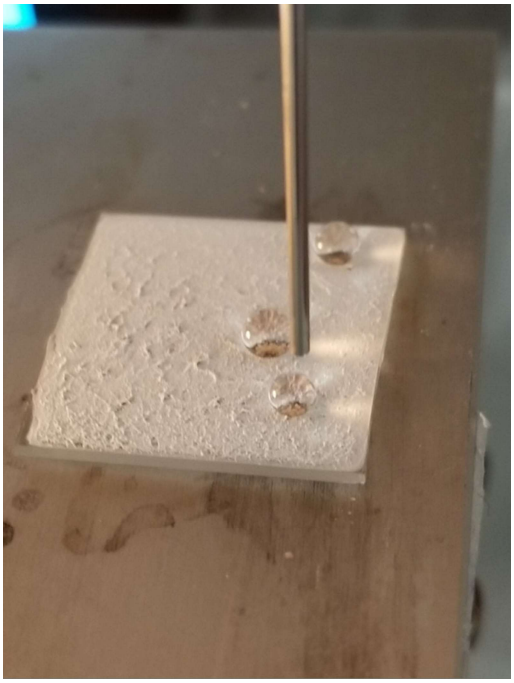

Figure 7 - Water droplets on a PVC Phase Separation surface

4c. PS/PMMA Selective Solvents

Another phase separation approach to producing hydrophobic polymer surfaces was proposed by Ma *et al*.[41] In this approach, a dissolved blend of polystyrene (PS) and poly(methyl methacrylate) (PMMA) is spin cast onto a glass substrate. While dissolved, these two polymers form a single phase, but separate into distinct polymer domains during spin casting. These substrates are then submerged in a selective solvent, re-dissolving the PS and leaving behind a hydrophobic, porous PMMA sponge.[41]

In an attempt to duplicate these results, a 7:3 blend of PS (Aldrich Chemical Company, Inc, Catalog Number 18242-7, Mw = 250kg/mol) and PMMA (Polysciences, Inc, Catalog Number 17913, Mw = 100kg/mol) was dissolved in THF(TCI, Product Number T2394) at a total polymer concentration of 50mg/mL. Once fully dissolved, 800µL of this solution was dispensed via pipettor onto glass microscope slides (25mm x 25mm) and spin coated (10s, 2000RPM). Once the THF had fully evaporated, the slides were dipped into cyclohexane (Fisher Chemical, Catalog Number C556-500) for up to 20 minutes to dissolve the PS. In one set of trials, 60°C cyclohexane was used, and in a second trial, room temperature solvent was used.

4d. Tuned Pattern Surfaces

Polydimethylsiloxane (PDMS) is frequently used to replicate microstructures for microfluidics, lab-on-a-chip and other research.[20] Liquid PDMS can be poured over a template and allowed to cure; when the cured PDMS is finally removed, it effectively copies the microstructure (inverted) of the original template. We used this same process in an attempt to fabricate hydrophobic surfaces using tuned, periodic patterns built by etching silicon wafers to produce a master template.

4d-1. Proof of Concept Trial

Pattern fabrication was accomplished through direct write photolithography using a Heidelberg DWL 66+ followed by plasma etching. The first pattern attempted utilized 10µm square holes, 10µm deep, spaced 10µm apart, as shown in Figure 8, below. When replicated with PDMS, this produced an inverted copy

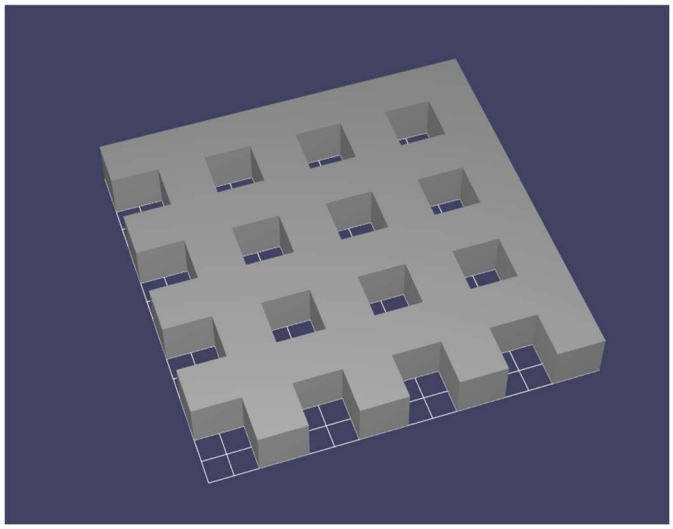

Figure 8 - Pattern layout used for first, proof of concept lithographc pattern

of this pattern - a surface composed of an array of pillars (sample PDMS-R0). Sylgard-184 (Dow Corning) was selected as our replication medium due to its widespread use. Sylgard-184 arrives as a two-part elastomer and, per the included instructions, is mixed in a 10:1 ratio (either by volume or by mass). The two parts were stirred vigorously by hand, and then placed in a vacuum chamber for 15 minutes to degas. After all the air had been removed from the liquid PDMS, it was poured over the etched silicon wafer and placed again into the vacuum chamber. During this second degas step, small air bubbles were observed to rise from the pattern holes, indicating that this is likely a necessary step when replicating these small features. After approximately 15 minutes, no additional air bubbles were observed and the PDMS was allowed to cure. One advantage of using Sylgard-184 is that it cures both thermally and at room temperature. Our first attempt at pattern replication used a thermal cure at 100°C for 45 minutes by

placing the silicon wafer and PDMS on a hotplate. However, this proved to be insufficient – when we attempted to remove the PDMS from the wafer, it remained strongly adhered to the silicon surface. Rather than risk damaging the master template or leaving PDMS residue behind on the etched pattern, the PDMS was allowed to continue to cure at room temperature for a total of 72 hours. After this long cure, the patterned PDMS was removed with little difficulty.

4d-2. Tuned Arrays

Following the successes in producing etched silicon wafer patterns and replicating those patterns with PDMS (Section 4d-1), additional test patterns were developed and a second master silicon wafer was produced. Due to the small size required for contact angle measurement and further testing, several patterns were able to be etched on a single silicon wafer. A total of eight different 25mm x 25mm patterns containing features ranging in size from 1µm to 3µm were designed for a 6" wafer. These features were divided into two general categories - checkerboard patterns (Figure 9, left) and free-standing pillars (Figure 9, right). In the case of checkerboard patterns, individual pillars would connect to neighboring pillars at each of their corners, leading to increased durability of the PDMS replication. For free-standing pillar patterns, each pillar would be surrounded by open space, leading to a lower contact area.

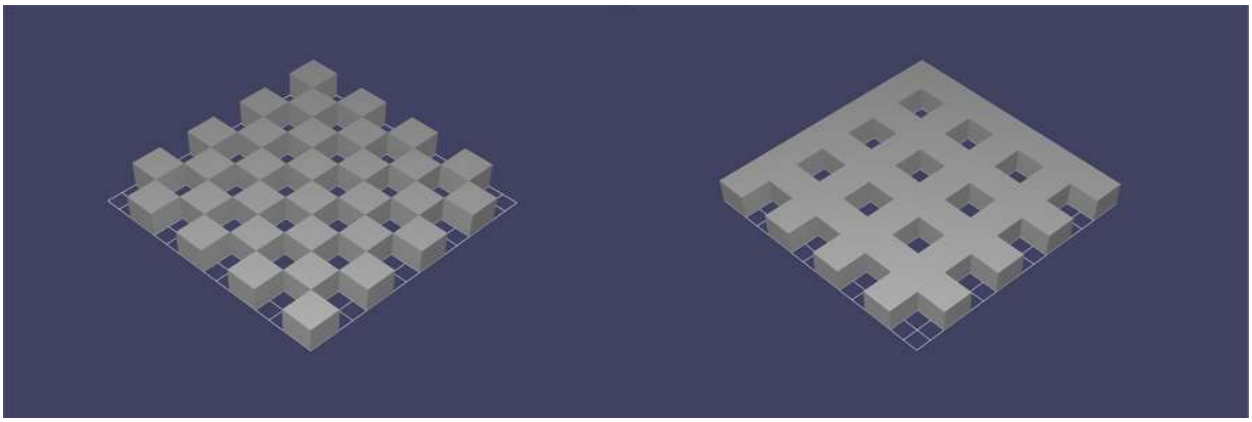

Figure 9 - Sample checkerboard (left) and free-standing pillar (right) patterns

The eight patterns selected for production, summarized in Table 3 below, included basic checkerboard and free-standing pillar patterns with 1µm, 2µm, and 3µm features/spacing, 1µm free-standing pillars with 1.5µm spacing, and round free-standing pillars with 2µm diameter. These patterns were manufactured using direct write photolithography with a Heidelberg DWL 66+ followed by plasma etching, as before, described in Section 4c-1, above.

Table 3 - Summary of hydrophobic patterns selected for production and testing

Name	Pattern Category	Feature Size	Feature Spacing
PDMS-R1	Checkerboard	1µm	1µm
PDMS-R2	Checkerboard	2µm	2µm
PDMS-R3	Checkerboard	3µm	3µm
PDMS-R4	Free-Standing Pillars	1µm	1µm
PDMS-R5	Free-Standing Pillars	1µm	1.5µm
PDMS-R6	Free-Standing Pillars	2µm	2µm
PDMS-R7	Free-Standing Pillars, Round	2µm	2µm
PDMS-R8	Free-Standing Pillars	3µm	3µm

One concern with reducing feature sizes from 10µm to 1-3µm involved the expected difficulty in demolding the replicated surface from the Silicon wafer master. During wafer production, all 8 patterns were etched to the same 10-12µm depth as before. Thus, as feature sizes were reduced, their already tall aspect ratio increased significantly. We were concerned that, during replication/de-molding, some features could tear from the bulk of the PDMS replica and become trapped within the master wafer. One solution was found within the field of microfluidics, coating the silicon wafer with a fluorinated silane to act as a mold release.[47]

To apply this silane coating, published procedures from the Harvard Microfluidics group were followed[30], and trichloro(1H,1H,2H,2H-perfluorooctyl)silane was ordered (Sigma Aldrich, Catalog Number 448931) and used. Our etched silicon wafer was first placed in a vacuum desiccator. Two to three drops of liquid Silane were placed on an aluminum foil dish in the desiccator. The desiccator was then closed, a vacuum

pump (Gast, Model DOA-P704-AA) was ran until a minimum pressure was reached, then, after sealing the desiccator, the pump was switched off. Gasses removed from the desiccator were pulled through a bed of potassium hydroxide to neutralize any hydrochloric acid vapor released during the attachment of the silane to the silicon wafer surface, as illustrated by Figure 10. The wafer and evaporating silane were left at reduced pressure for 30 minutes. The wafer was then removed from the desiccator and heated at 150°C for 10 minutes on a hotplate to drive off any excess silane, and then was ready for use/replication.

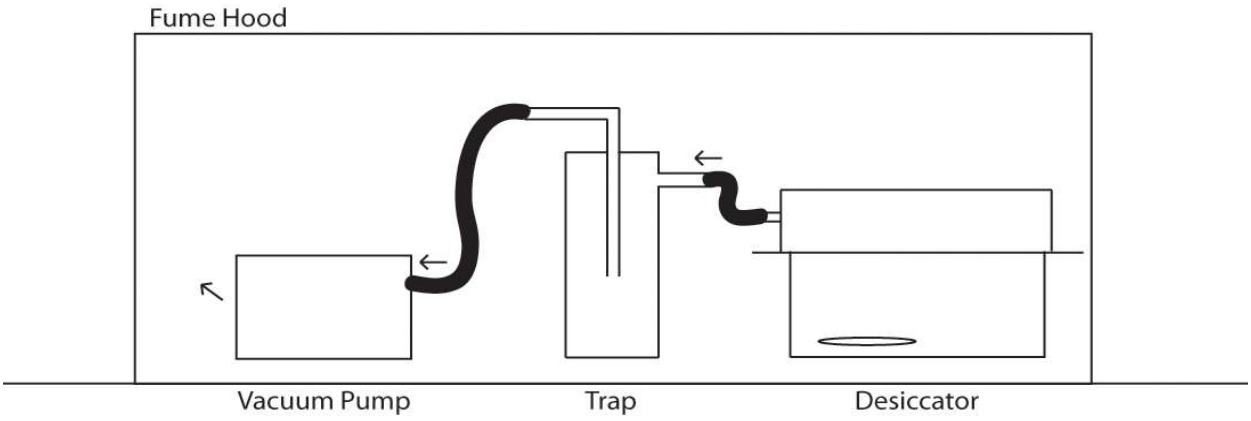

Figure 10 – Apparatus setup for the application of silane coatings

Replication of these patterns was accomplished using Sylgard-184 (Dow Corning), mixed and prepared per the included instructions and poured over the etched silicon wafer. Modeling clay was used as a berm to contain the liquid Sylgard, allowing for a thicker, more durable layer to be applied. Immediately after pouring, the silicon wafer was placed in a vacuum desiccator to degas and to remove any air pockets trapped in the etched pattern, between the wafer surface and liquid Sylgard. The wafer was then left to cure at room temperature for 72 hours before de-molding. This PDMS sample contained replications of both our desired etched patterns as well as a "replication" of the polished flat silicon wafer surface. This flat replication was used for baseline measurements to ensure that any unexpected transfer of silane to the sample does not impact our results.

4e. TIPS Process

Surfaces were produced through a range of variations of TIPS process parameters; however, all trials followed the same general procedures. To ensure consistency in our results, the same polymer and solvents were used for all trials.

As a general procedure, PMMA was first weighed and added to an ethanol/water solvent mixture. This mixture was then covered and placed on a 60°C hotplate, under strong magnetic stirring, for several hours, until the PMMA had fully dissolved. After all of the polymer had fully dissolved, the magnetic stir

bar was removed and the polymer solution was allowed to cool and precipitate. As the solution cooled, the clear solution first became white and opaque as the polymer precipitated into a colloid; over time, this precipitate settled/collected on the floor of its container, forming our hydrophobic surface. After being left to precipitate overnight, excess ethanol/water/polymer solution was decanted and discarded. The remaining surface was finally allowed to fully dry, uncovered, in a fume hood for approximately 24 hours.

While determining ideal experimental conditions to produce these surfaces, several parameters were varied. Experiments were performed varying the concentration of dissolved PMMA, the molecular weight of PMMA used, and the cooling rate/temperature. Contact angle measurements and abrasion tests were performed on both free-standing surfaces (produced in glass containers) and on surfaces adhered to a polystyrene substrate (produced in petri dishes). As-produced, free-standing surfaces were cut into smaller samples for testing using scissors or a razor blade. Surfaces produced on a PS substrate were cut into 0.75 inch (1.9cm) squares using a band saw prior to testing.

4f. Replicating TIPS Process with Hansen Solubility Parameters

Our general method for testing this theory/approach was to begin with small scale tests. A pair of solvents were selected such that the solvent blend's HSP values were each greater than the polymer's HSP values; ratios of the two solvents were selected so various blends tested would fall at a range of distances from the polymer. 0.1g of a given polymer was measured and added to a total of 10mL solvent blend and left at room temperature for 48 hours to verify insolubility at room temperature. Samples which did not dissolve at room temperature were then heated to approximately 10°C below the boiling point of the more volatile solvent in the blend. Solutions which dissolved at this elevated temperature were then moved to the lab refrigerator (10°C) or freezer (0°C) to rapidly cool, with the intent of reprecipitation and subsequent sedimentation/self-assembly and solvent sintering in a "single pot" process.

4g. Sintered Microparticle Surfaces

Our next approach to replicate the TIPS process using additional polymers was to deconstruct the overall process into its individual steps. By first forming appropriately sized microparticles, then sintering the particles together, the resulting surface should have similar topography as TIPS process surfaces. Additionally, by taking this "separate steps" approach, we can maintain greater control over the exact size

of microparticles used and the degree or extent of sintering performed. By controlling these two parameters, a balance between enhanced surface hydrophobicity and surface durability can be found.

To produce these sintered microparticle surfaces, polymer microparticles were first produced through a single emulsion/solvent evaporation process, described below in Section 4g-2. These microparticles were then isolated and sorted by size via vacuum filtration, described in Section 4g-3. After the microparticles were isolated, they were sintered together to form a cohesive surface through a solvent sintering process, as described in Section 4g-4.

4g-1. PMMA Proof of Concept

These sintered microparticle surfaces were first produced from PMMA as a proof of concept. This allows for a direct comparison of surfaces produced through this sintering process to well-understood TIPS surfaces (described in Section 4e, above).

Microparticles were produced by first dissolving PMMA in a hot ethanol (Deacon Labs, Product Number 2716GEA)/water (Barnstead E-pure system) solution, as in the TIPS process, described above. After the PMMA had fully dissolved, the solution was again cooled in a refrigerator. For this sintered microparticle surface proof of concept, the dissolved polymer solution was stirred continuously during cooling to prevent sedimentation, while still allowing for precipitation and microparticle growth. This was accomplished by moving the hot, dissolved polymer solution and stir plate into a large, walk-in cooler (also set to 10°C) overnight. Dispersed microparticles were then collected via vacuum filtration and dried in air.

After the microparticles were collected, they were sintered together to form a hydrophobic surface. The sintering solution was composed of acetone (a good solvent for PMMA) and hexane (a non-solvent for PMMA). Acetone is a highly volatile solvent (vapor pressure = 30 kPa) which quickly dissolves PMMA, while hexane is somewhat less volatile (vapor pressure = 17.6 kPa), is miscible with acetone, and is a non-solvent for PMMA. Our sintering solutions consisted of varying concentrations of acetone (Macron, VWR Catalog Number MK244002) in hexane (JT Baker, n-Hexanes, Item Number 9304-02), ranging from 10% v/v to 35% v/v acetone. To produce surfaces, 0.2g PMMA microparticle powder was placed in a 50mL beaker, forming a thin, even layer. To this, 1mL of sintering solution was added, enough to evenly wet all of the PMMA powder. This was then placed into a fume hood and allowed to completely evaporate.

4f-2. Single Emulsion/Solvent Evaporation Process

Several existing methods for forming polymer microparticles/nanoparticles were identified in the literature.[14,17,18] The most promising and feasible method was Sharma *et al*.'s Single Emulsion Solvent Evaporation process[18]. In this process, polymer dissolved in an organic solvent is added dropwise to a stirred poly(vinyl alcohol) (PVA) /water solution. By selecting a solvent which is immiscible with water, the mixture forms an emulsion of droplets of dissolved polymer suspended in PVA/water when stirred. The solvent evaporates as the mixture continues to stir and the droplets solidify, forming the microparticles.

Two parameters were varied to control the size of the resulting polymer microparticles – concentration of polymer dissolved in organic solvent, and emulsion stirring speed. Our first experiments were designed to construct a pair of "calibration curves" to correlate measured microparticle diameter to these two experimental parameters. One set of experiments varied the concentration of polymer dissolved in organic solvent at a fixed stirring speed, and a second set of experiments varied the emulsion stirring speed at a fixed polymer concentration.

Our various experiments first required the preparation of two solutions, dissolved polymer and 1wt% PVA/water. For the PVA solution, 1g PVA (Scientific Polymer Producs, Inc, Catalog Number 352, Mw = 16kg/mol, 98% hydrolyzed) was weighed and added to 100mL deionized water (Barnstead E-pure system) in a beaker. This solution was then heated to near boiling (~90-95 °C) and stirred overnight. We found that covering and wrapping the beaker with aluminum foil helped speed up dissolution of the PVA and minimized evaporation losses. For the dissolved polymer solution, we selected Ultem 1010 (3DXTech, Ultem 1010 3D Printing Filament) as our polymer and chloroform (Macron, VWR Catalog Number CAMK444004) as our immiscible solvent. 1-5g Ultem (depending on the trial being run) and a small stir bar were added to 25mL chloroform in a sealed vial. This solution was then allowed to stir until the Ultem had completely dissolved – 2-3 hours if also heated to 40°C, or overnight if left at room temperature. Once both solutions were completely dissolved, they were cooled to room temperature before proceeding.

To produce the emulsion/microparticles, dissolved polymer was added dropwise to an equal volume of vigorously stirred PVA/water solution. During our initial trials to produce calibration curves, 25mL chloroform/Ultem solution was added dropwise using a separatory funnel to 25mL 1 wt% PVA/water in a 150mL beaker. During one set of experiments, the dissolved polymer concentration was varied from 1g Ultem/5mL chloroform to 1g/25mL and all trials were run at 1000 RPM stir speed. For the second set of experiments, the stirring speed was varied from 600 – 1400 RPM and all trials were run at 1g/20mL.

After the two solutions had been combined, the mixture was stirred for approximately 24 hours before proceeding, allowing all solvent (chloroform) to evaporate, solidifying the Ultem microparticles.

During our first (calibration curve) runs, the resulting microparticles were isolated and washed with deionized water using simple vacuum filtration with 1µm filters (VWR Glass Microfiber Filters #696). These dried particles were then sputter coated, imaged via SEM and analyzed with FIJI (https://imagej.net/Fiji) to determine particle sizes. Through this FIJI software, images can be quickly analyzed to identify all particles in the image and calculate their size. From this data (described in Section 6g), we were able to assemble our calibration curves and better predict resulting microparticle average sizes. Extrapolating from this data, we selected 1g Ultem/20mL chloroform stirred at 1600 RPM as our final parameters to "mass produce" our microparticles for sintering and surface testing.

As an alternative to magnetic stirring, we also attempted to produce microparticles using a bath sonicator (VWR Model 75D). In a small-scale trial, 5mL Ultem/Chloroform solution was added dropwise (using a micropipettor) to 5mL 1% PVA/water in a vial suspended in the sonicator bath. However, the sonicator was not powerful enough to produce the same emulsion as before, and the two liquids simply separated into layers. We also investigated the use of a probe sonicator, but, did not run any trials. We posit that this approach can (based on power level settings) produce significantly smaller microparticles (or nanoparticles).

4g-3. Microparticle Filtration/Size Separation

Once our microparticles had been produced and all solvent evaporated from the solution, we focused on isolating these microparticles and separating them by size. We were most interested in particle sizes ranging from 1-5µm and from 5-10µm. To accomplish this separation, we used a multi-stage filtration process. Unfortunately, this step was the source of the majority of issues and challenges we faced during this work. We hypothesized that, by using a series of filter papers - 10µm (Whatman #93), 5µm (VWR Cat#28310-015), and 1µm (VWR Glass Microfiber Filters #696) pore sizes, we would be able to effectively and efficiently segregate our produced microparticles through vacuum filtration into >10µm, 5-10µm, 1-5µm, and <1µm "bins" as shown in Figure 11. However, this process did not proceed as smoothly as we had initially assumed.

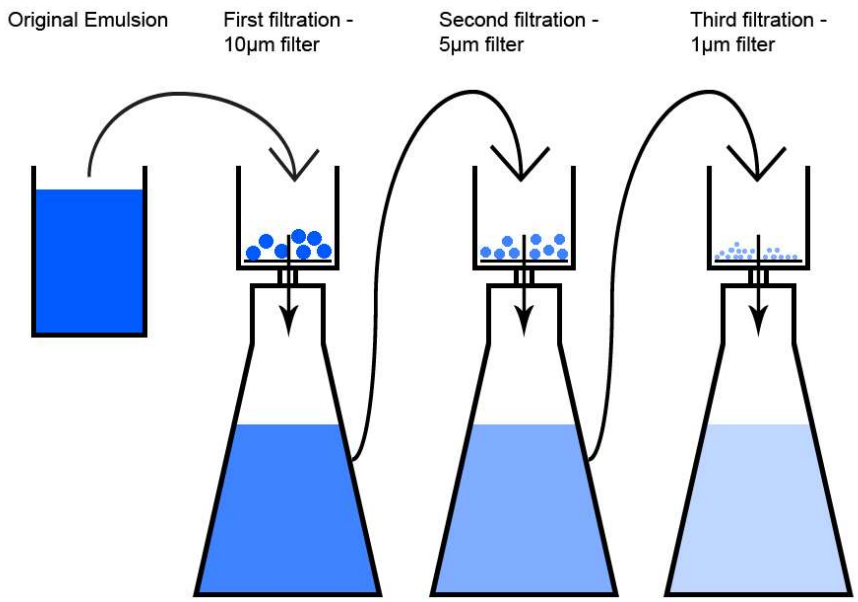

Figure 11 - Each filtration step retains progressively smaller particles, allowing us to collect "bins" of particle sizes

Prior to filtration, 50-75mL of boiling water was added to the microparticle/PVA solution. This was stirred for 5 minutes to ensure that all PVA was fully dissolved and would not be retained during any filtration steps. The slurry was then filtered through a 10µm filter paper. The filtrate (now containing only microparticles with diameters less than 10µm) was retained for additional filtration and separation while the filter paper and retained (10µm+ diameter) microparticles were discarded. The retained filtrate was then filtered a second time using a 5µm filter paper. After this step, both the filtrate and filter paper/retained particles were saved. Finally, the filtrate was filtered a third time using a 1µm filter paper. The filter paper and retained microparticles were saved, and the filtrate was discarded. The two saved filter papers (containing the desired 1-5 and 5-10µm particles) were dried in air before proceeding further. After the microparticles (and filter papers) had fully dried, they needed to be removed from the filter paper before they could be formed into a hydrophobic surface. This was attempted in several different ways before arriving at an effective solution. Our first attempts were done by simply scraping the particles from the filter using a scoopula. While moderately effective, this process often introduced contamination to our final products in the form of filter paper fibers and typically was unable to remove all particles from the filter. However, by placing the dry filter paper into a large beaker and adding a small, arbitrary amount of boiling water and gently agitating the filter paper, the vast majority of particles were effectively removed with minimal paper fiber contamination. Once the microparticles were successfully removed from the filter papers, the water and microparticles were boiled dry on a hotplate and the microparticles were finally collected.

4g-4. Solvent Sintering

Once we had separated the produced microparticles into the two desired size "bins" (5-10µm and 1-5µm), our next goal was to sinter them into a cohesive, durable, hydrophobic surface with morphology similar to that of our TIPS surfaces produced earlier, as shown in Table 12. To accomplish this, we used two different approaches – sintering with a liquid solvent/non-solvent blend (described above in Section 4f-1) and sintering with solvent vapor. In both approaches, a balance between surface strength (through large, strong interconnections between particles) and surface hydrophobicity (through high surface roughness and small interconnections) must be found.

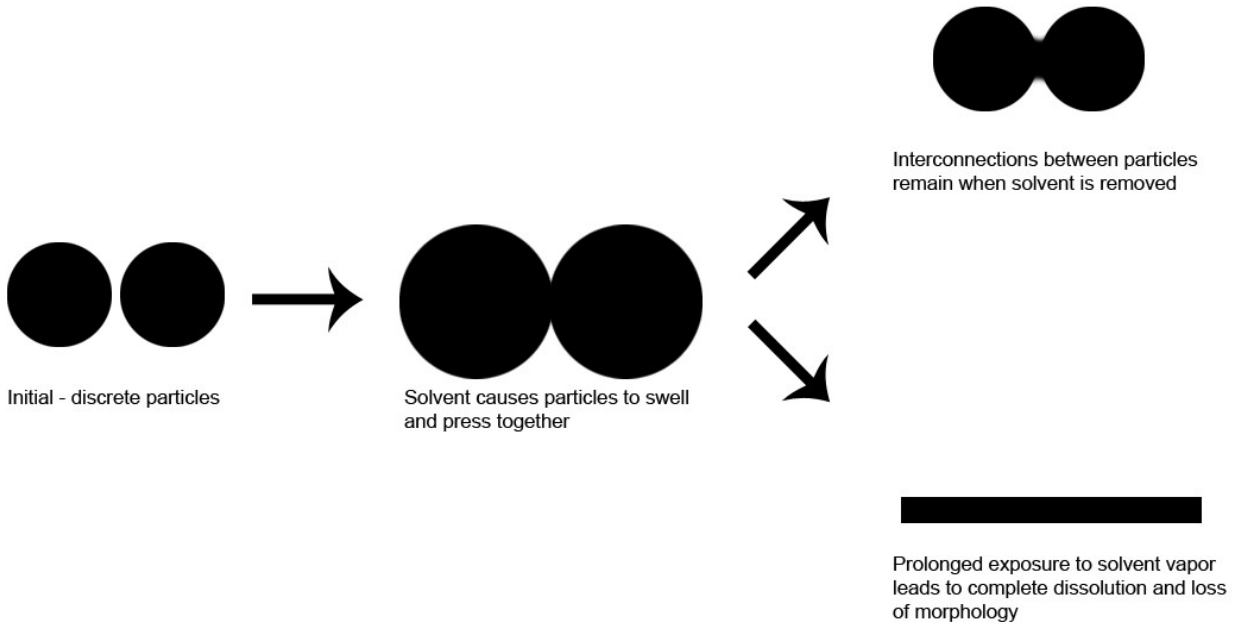

Figure 12 - Solvent sintering process

The liquid solvent/non-solvent sintering was based off work done by Brown, *et al*.[12]. In this work, the authors used solvent/non-solvent blends to sinter polymer microparticle scaffolds, resulting in TIPS-like interconnected particle networks, as described in Section 6e, below.

As an alternative process, we also investigated using solvent vapor to perform the necessary sintering. By exposing the polymer microparticles to a solvent vapor atmosphere, we hypothesized that we could achieve the same end result as with our TIPS process and Brown's group. Rather than varying the "good solvent" concentration of the sintering solution to control the degree of sintering, this solvent vapor process is similarly controlled by the duration of solvent vapor exposure.

We hypothesized that the same sintering process which forms interconnections between particles could be used to also form interconnections with a similar polymer base layer that would act as a substrate for the microparticles. To test this hypothesis, we first spin coated glass slides with a thin layer of Ultem. Ultem (3DXTech, Ultem 1010 3D Printing Filament) was dissolved in chloroform (Macron, VWR Catalog Number CAMK444004) at a concentration of 1g Ultem/5mL chloroform. 0.4mL of this solution was dispensed via micropippettor onto a 25mm x 25mm piece of glass microscope slide and spun at 1000 RPM for 45 seconds. Loose microsphere powder (either 5-10μm or 1-5μm) was scooped onto the spin-coated glass, then pressed flat with a second coated glass slide to form our initial sintering test samples.

Sintering of these samples we accomplished in a vacuum desiccator. The desiccator was placed into a fume hood, then loaded with the sample to be sintered and a small beaker of liquid solvent. For our Ultem microparticles, chloroform was used as the solvent and 20-30mL was added to a 50mL beaker inside the desiccator. This volume of solvent represents a significant excess, which was used for all trials to ensure full saturation of the chamber atmosphere. Additionally, the same 50mL beaker was used for all trials to ensure the rate of solvent evaporation remains as consistent as possible from run to run. After both the sample and solvent were loaded into the desiccator, the desiccator was closed and evacuated using a (Gast, Model DOA-P704-AA) vacuum pump. The pump was allowed to run for 3 minutes, then the desiccator was sealed, and the pump was turned off. The duration of sintering was varied from run to run to observe the changing morphology of the surfaces produced and to determine ideal sintering durations to optimize both surface hydrophobicity and durability. Durations of 30 minutes to 2.5 hours were tested. Sintering was ceased by slowly re-opening the vacuum desiccator valve, refilling the atmosphere inside, and removing the sample. Samples were allowed to stand in a fume hood overnight before further testing, to ensure the complete evaporation of any residual solvent

5. Instrumentation

5a. Contact Angle Measurements

Contact angle measurements were performed using a goniometer (Ramé-Hart Model 250). Deionized water (Barnstead E-pure system) was used as a test liquid, 5μL droplets were dispensed using a pipettor and were placed on the surface by hand. A series of either three or five droplet measurements were taken per sample, contact angles were measured using DROPimage and the average measurement of 10 readings per droplet is reported.

5b. Abrasion Testing

While contact angle measurements could be accomplished using standardized methods and commercially available (and available to our research group) equipment, additional tests on these surfaces necessitated the development of a custom testing apparatus. To measure durability, renewability, and to simulate wear on these surfaces, a series of abrasion tests was needed. A cost-effective solution could be developed in-house, which would allow us to fine tune the performance and aggressiveness of the testing. Taking cues from commercially available testing solutions, like the Gardner Heavy Duty Linear Abraser 5800, and from other experimental methodology, similar to those used by Wang, *et al*.,[39] we formulated our own testing process.

As a general procedure, sandpaper would be pulled across the test surface. By varying the number of abrasion cycles, different amounts of surface wear could be tested. For reproducibility, a standardized 250g mass and a consistent abrasive (600 grit sandpaper) was used for all tests. To also maintain a consistent sandpaper travel rate, a small DC electric motor was used to pull the sandpaper across the test surface, powered by a variable power supply (GW Instek GPS-3030) set to a constant 10V. As shown in Figure 13 below, the motor was mounted to a flat base. A cord was attached to the spindle and a standard binder clip which was used to hold the sandpaper for testing. The 250g mass was placed on top of this sandpaper to apply constant pressure from run to run.

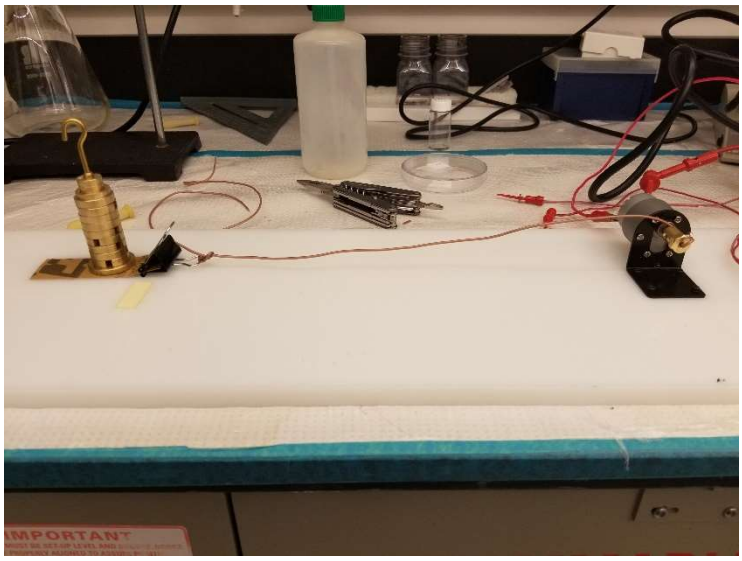

Figure 13 - Abrasion testing apparatus with 250g test mass

Free-standing test surfaces were mounted onto glass microscope slides using double sided tape for testing. These slides were then mounted onto the apparatus base plate using additional double-sided tape. Test surfaces produced on PS petri dishes were mounted directly to the apparatus base with double-sided tape for testing.

For each test cycle, the 250g mass was placed on the 600 grit sandpaper and pulled across the test surface at a rate of approximately 2cm/second. After the sandpaper had completely passed across the test surface, the electric motor was turned off and the test was reset. For consistency of wear, the sandpaper was replaced after every five abrasion cycles. To verify the reproducibility of this procedure, tests were conducted on a total of 6 surface samples. Contact angle measurements were taken after 1, 5, 10, 15, and 20 abrasion cycles for each surface.

5c. Surface Imaging

Samples were examined via standard optical microscopy and by scanning electron microscopy, using a Hitachi S-4000 Scanning Electron Microscope (SEM). While optical microscopy allowed us to see the general surface morphology of our samples, use of the SEM allowed us to view how changes in polymer molecular weight and concentration changed this morphology in higher resolution. Due to the electrically insulating nature of PMMA, clear images of the surface were difficult to obtain and were frequently distorted due to charging effects. These effects were minimized by reducing the SEM acceleration voltage to 2.0-3.0 keV. Image quality could be further improved by sputter coating a thin metal layer over the samples. After obtaining access to improved equipment, later samples were imaged using a

TESCAN SEM after sputter coating with gold. This led to significant improvements in image resolution, both through the reduction of charging effects and by enabling higher acceleration voltages to be used.

Atomic Force Microscope (AFM) scanning of the samples was also attempted but proved to be unsuccessful. It is believed that our surfaces were simply too rough (micron-scale changes in surface topology) for effective measurements to be taken with the equipment available to us.

5d. Silicon Wafer Processing

Silicon wafer processing was done in partnership with the RIT SMFL (Semiconductor and Microsystem Fabrication Lab). Silicon wafers were first coated with AZ MIR-701 positive photoresist and baked using an SVG 88 wafertrack. (Direct) Lithographic writing of our test patters was accomplished using a Heidelberg DWL 66+ Laser Writer. The exposed photoresist was developed using Microposit MF CD-26, again on the SVG 88 wafertrack. Etching was done to a depth of 12-15μm using an STS ASE Deep Silicon Etch with C_4F_8, SF_6, O_2 and Ar process gasses. Final removal of remaining photoresist was then accomplished thermally, in an oven.

6. Results and Analysis

6a. Baseline Samples and Measurements

In order to assess the specific impact of surface structure on hydrophobicity, we needed to first determine the baseline contact angles for flat surfaces. Therefore, we measured contact angles of flat, spin coated surfaces of PS, PMMA, and Ultem. These initial experiments also allowed us to verify the reproducibility of goniometer measurements since the spin-cast samples were expected to be uniform from surface to surface. These initial experiments would enable us to develop sufficient expertise in using the equipment. After experimenting with different solvents and spin coater settings (RPM and spin duration), we found baseline contact angle measurements of 66.1°±1.5° for PMMA, 85.6°±1.5° for PS, 70.0°±1.1° for Ultem, and 116.1°±1.6° for PDMS, as shown in Table 4, below. These values all generally agree with previously published literature values.

Table 4 - Baseline contact angle measurements

Sample	**Contact Angle (°)**	**Standard Deviation (°)**	**Literature Values (°)**
PMMA-flat	66.1	1.5	68[41]
PS-flat	85.6	1.5	84[48]
Ultem-flat	70.0	1.1	64[49]
PDMS-flat	116.1	1.6	116.7[50]

6b. PVC Phase Separation

Surfaces produced through PVC phase separation (as described in Section 4a, above) showed a very high contact angle (154.4°±1.4°) but proved to be extremely fragile. After the contact angle measurement, using a tissue to remove the water droplet would also brush away and destroy the hydrophobic PVC surface. Additionally, when samples of this surface were subjected to our abrasion testing process, described in Section 5b, above, the entire surface was removed from the glass slide upon the first abrasion cycle. Changes to the volume of polymer dispensed (varying between 300-800µl, as shown in Table 5) changed contact angle results slightly, these changes did not improve surface durability. While contact angle measurements for these PVC surfaces were extremely high, poor durability prevented significant study of this approach.

Table 5 – PVC surface contact angle results

PVC Solution Dispensed (µl)	Contact Angle (°)	Standard Deviation (°)
300	150.4	4.8
400	146.6	1.2
500	145.2	2.0
600	147.2	2.2
800	154.4	1.4

The poor durability of these PVC surfaces could be explained by poor interparticle bonding. As the solution evaporates, the continued presence of ethanol (a non-solvent for PVC) leads to phase separation into a polymer-rich THF phase and a polymer-poor ethanol phase. As the THF continues to evaporate and the total volume decreases, separate polymer-rich domains are brought closer together. As the remaining THF evaporates, these polymer-rich domains solidify. However, the remaining ethanol forms voids in this polymer matrix, minimizing contact between separate polymer-rich domains. This allows for only limited interaction between separate particles or domains, and prevents the formation of a uniform smooth surface or strong interconnections between particles.[40]

The porosity of these hydrophobic PVC surfaces also diminishes their durability. Based on contact measurements, Chen, *et al*. calculated that the porosity of these surfaces was as high as 88.5%. Additionally, published micrographs of these surfaces indicate that precipitated particles are smaller than 500nm in diameter.[40] A small particle size prevents the formation of large, strong interconnections between particles and a large air volume within the surface drives those particles apart, further weakening interconnections. The high roughness that this network or matrix of nanoparticles offers is very advantageous for increasing the hydrophobicity of the surface, but also significantly limits the durability of these networks.

6c. PS/PMMA Selective Solvents

When PS and PMMA are dissolved together in THF, the two polymers intermix and form a homogenous solution. However, as Ma *et al*. note, PS more readily dissolves in THF than PMMA does.[41] This difference in solubility leads to phase separation as the solvent evaporates. The less soluble PMMA begins to precipitate from solution, leaving behind a PS-rich liquid phase. By spin coating this solution the solvent is driven from solution quickly and the two polymer phases separate to form a complex matrix of PMMA with pores of PS.

Ma *et al.*[41] reported that these surfaces could be made hydrophobic by using a selective solvent to dissolve and remove the PS pores, without disrupting or destroying the PMMA matrix. After using cyclohexane to dissolve PS, the remaining PMMA matrix provides sufficient surface roughness to dramatically increase the surface's contact angle.[41] The authors report dissolving the PS phase by exposing the spin-cast sample "to enough cyclohexane at 70°C for 20 min."[41]

When these procedures were repeated, the spin-cast films appeared similar to Ma *et al.*'s results[41] and were transparent and visually uniform. However, when our spin-cast films were submerged in an excess of cyclohexane, heated to 60°C on a hot plate, for 20 minutes, both polymers (PS and PMMA phases) had been nearly fully removed from the glass substrate. Droplets of water placed on these substrates immediately spread, wetting the surface – the selective solvent treatment had decreased the hydrophobicity of the surface when compared against flat, untreated PMMA.

Additional spin-cast films were produced and were exposed to cyclohexane for progressively shorter times. This culminated in a series of trials using soak times of 5, 10, 20, and 30 *seconds* rather than *minutes*. These trials were conducted with both heated solvent (heated to 60°C on a hotplate) and with room temperature solvent. As shown in Figure 14, below, the surfaces reached a maximum contact angle of 89.0°±2.3° (as shown in Table 6, below), still much lower than the 154.3°±3.9° reported by Ma *et al.*[41]

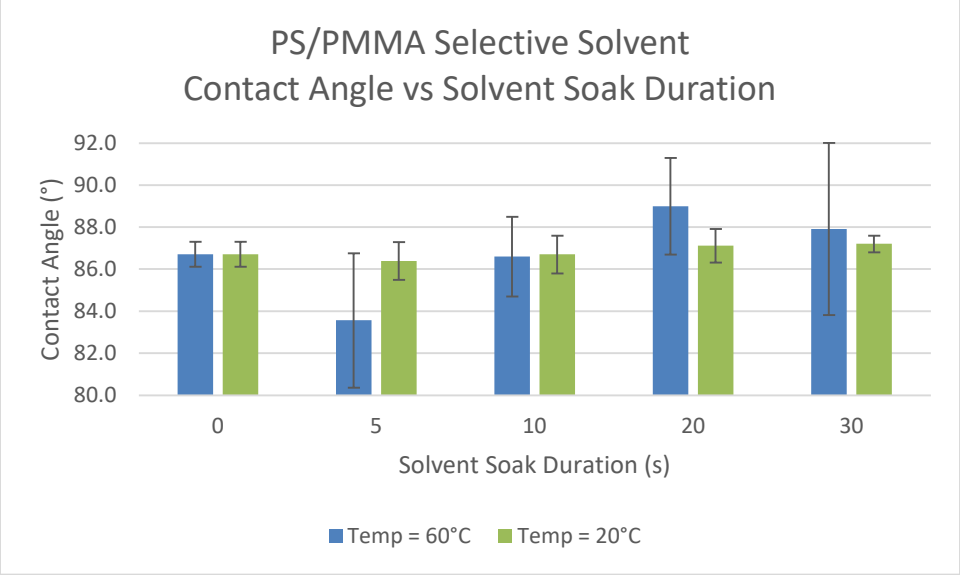

Figure 14- Contact angle measurements from PS/PMMA selective solvent surfaces at varying solvent soak durations

The significant variance in results between our work and those published by Ma *et al.* in terms of contact angle measurement (89.0°±2.3° vs 154.3°±3.9°) and in ideal solvent soak duration (20 seconds vs 20 minutes)[41] could be explained by differences in polymer molecular weights used. While the same ratio of

polymers by mass was used in all experiments, our work used 100 kg/mol PMMA and 250 kg/mol PS while Ma *et al*. used 93.9 kg/mol PMMA and 194.9 kg/mol PS.[41] These different molecular weight values (both in terms of absolute value and ratio between molecular weights) may have led to the formation of larger PS pores within the PMMA matrix. Once these pores dissolved away in the cyclohexane, larger surface voids may have caused water droplets to fall into a Wenzel wetting state, rather than the Cassie-Baxter state as in Ma *et al*'s report. However, due to the small relative difference in molecular weights, this is unlikely to be the sole cause. Other factors such as differences in polymer tacticity, polydispersity, and degree of crystallinity of the cast polymer films can also affect the morphology and solubility of the polymers and may have also contributed to the differences in results between our experiments and those reported in the literature.[41]

Table 6 – Contact angle measurements for PS/PMMA surfaces under varying solvent soak conditions

Sample Name	**Soak Duration (seconds)**	**Solvent Temperature (°C)**	**Contact Angle (°)**	**Standard Deviation (°)**
PS/PMMA-0	0	N/A	86.7	0.6
PS/PMMA-5c	5	20	86.4	0.9
PS/PMMA-10c	10	20	86.7	0.9
PS/PMMA-20c	20	20	87.1	0.8
PS/PMMA-30c	30	20	87.2	0.4
PS/PMMA-5h	5	60	83.6	3.2
PS/PMMA-10h	10	60	86.6	1.9
PS/PMMA-20h	20	60	89.0	2.3
PS/PMMA-30h	30	60	87.9	4.1

6d. Tuned Pattern Surfaces

Tuned pattern surfaces were produced by first producing an etched silicon wafer using photolithographic processes (Section 4d), then replicating these etched patterns using liquid polydimethylsiloxane (PDMS). Once this PDMS cures, it can be demolded from the silicon wafer to reveal an inverted copy of the original pattern. Contact angle measurements were then taken of each sample, discussed below, and compared against contact angle measurements of flat PDMS. These experiments allowed us to examine the impact of various surface patterns on the hydrophobicity of the surface, independent of surface material. These measurements were also compared against predicted Cassie-Baxter state contact angles, which allowed us to compare real-world performance of these surfaces and patterns to theoretical, ideal performance.

6d-1. Proof of Concept Trial

Our work with etched silicon wafers and PDMS replication began with a proof of concept trial. The selected pattern utilized relatively large 10µm x 10µm x 10µm features spaced 10µm apart. These features were etched into the silicon wafer surface and the (inverted) PDMS replication of this pattern consisted of 10µm square pillars.

Contact angle measurements were taken from both a flat, non-patterned sample of PDMS and our replicated pattern (sample PDMS-R0). The flat PDMS sample resulted in an average contact angle of 116.1°±1.6° and served as our reference point for these experiments. The PDMS-R0 sample resulted in average contact angle measurements of 106.6°±3.6°, a decrease in contact angle versus flat/non-patterned PDMS. This indicated to us that the pattern features were too large to effectively form a hydrophobic surface, but that pattern replication at this small size scale was possible. Following this success of our process, we designed new patterns and etched a new silicon wafer containing a total of 8 additional test patterns.

6d-2. Tuned Arrays

For our second round of experimentation and testing, we designed and produced a wider range of patterns which fall into one of two general categories – checkerboard patterns and free-standing pillar patterns. For each pattern, predicted contact angles were calculated (Cassie-Baxter state), actual contact angles were measured, and SEM images were taken of the surface and compared to the expected pattern. Contact angles were compared against measurements of flat PDMS, 116.1°±1.6°.

Checkerboard Patterns

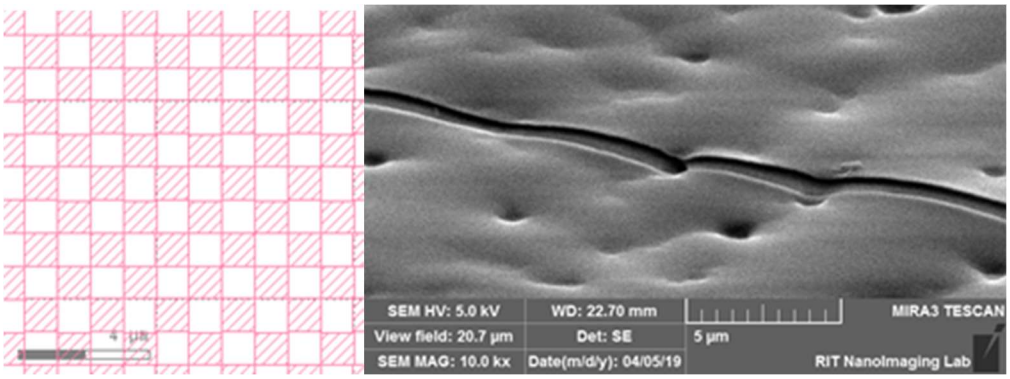

Figure 15 - 1µm checkerboard pattern. Designed pattern (left), SEM image of sample PDMS-R1 (right)

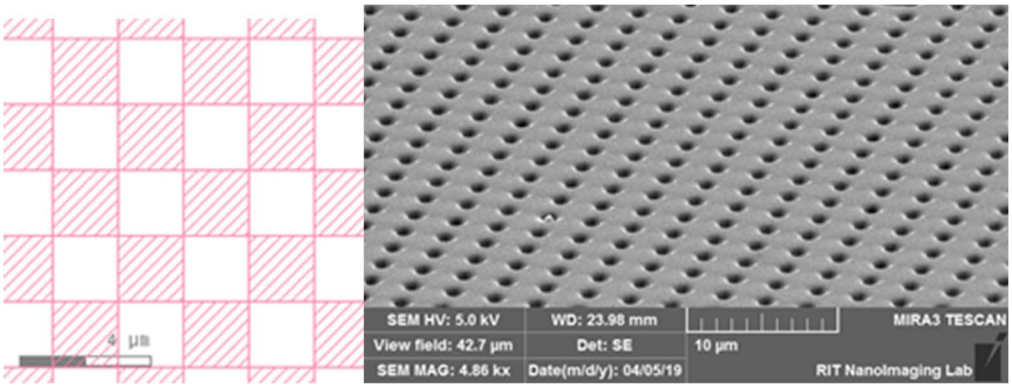

Figure 16 - 2µm checkerboard pattern. Designed pattern (left), SEM image of sample PDMS-R2 (right)

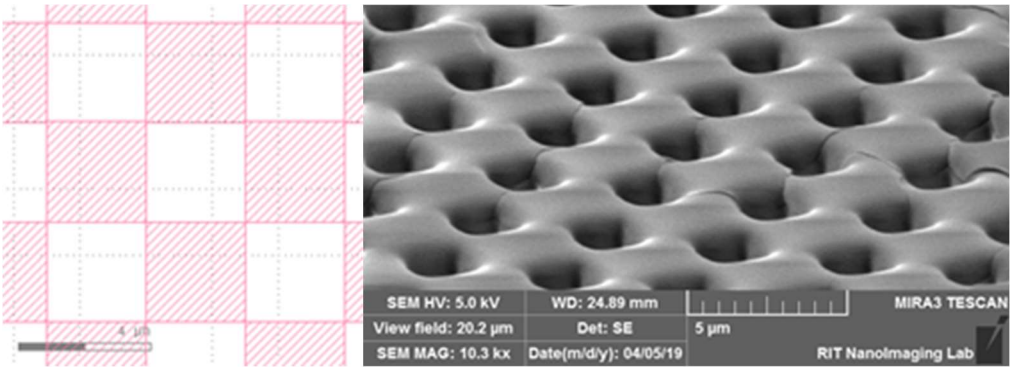

Figure 17 - 3µm checkerboard pattern. Designed pattern (left), SEM image of sample PDMS-R3 (right)

The first and smallest pattern, a 1µm checkerboard, pushed the limits of our lithography resolution. The Heidelberg DWL 66+ was run using a 4mm printhead, capable of producing features as small as 0.8µm. Our designed pattern required features only slightly larger than this minimum. This was further complicated by the specific shapes used in our pattern – the Heidelberg struggled to reproduce the crisp corners required by these patterns. This was most apparent at the smallest 1µm feature sizes but did impact the production of all patterns. Between this inaccuracy in production and the high viscosity of the liquid PDMS used, replication of this first pattern (sample PDMS-R1) resulted in a gently undulating surface, rather than an array of pillars and gaps (as shown by Figure 15) and a much lower than expected contact angle due to this decreased roughness, as shown in Figure 23 and summarized in Table 7, below.

The second pattern, using larger 2µm features was reproduced more accurately by the Heidelberg. However, too much silicon was removed during etching. This resulted in a replicated surface comprised of lines of small holes (as shown in Figure 16), not a checkerboard of equally sized pillars and voids, as intended. These pillars had much larger interconnections than desired and designed, resulting in increased contact area between droplets and the surface, and a lower contact angle than predicted.

Our third pattern, utilizing 3µm features, was reproduced by the Heidelberg most accurately, however interconnections at the corners of each feature were still larger than intended, as shown in Figure 17. This again led to a larger-than-intended contact area between the liquid droplet and the PDMS surface.

Free-Standing Pillar Patterns

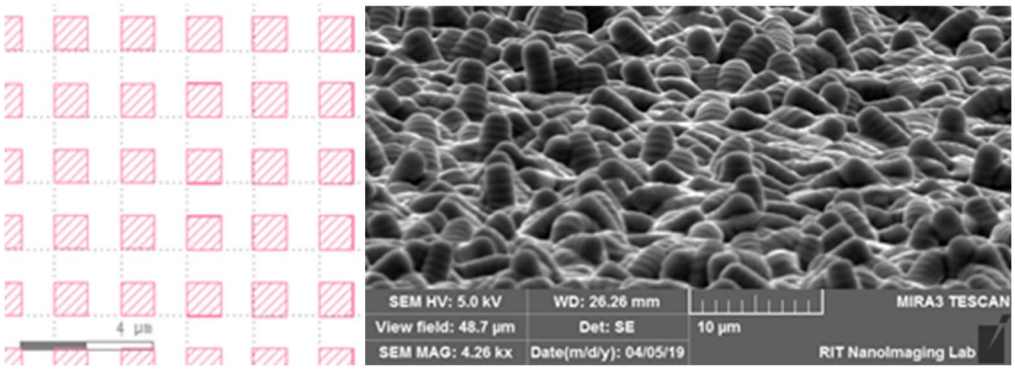

Figure 18 - 1µm freestanding pillars pattern. Designed pattern (left), SEM image of sample PDMS-R4 (right)

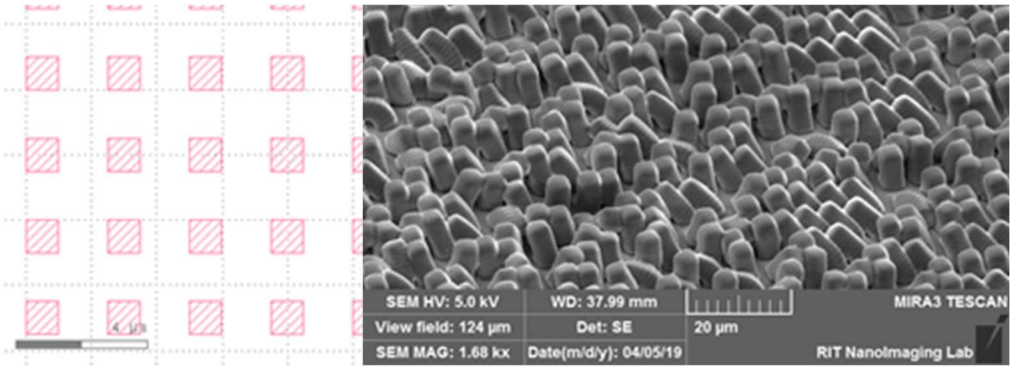

Figure 19 - 1µm free-standing pillars with 1.5µm spacing. Designed pattern (left), SEM image of sample PDMS-R5 (right)

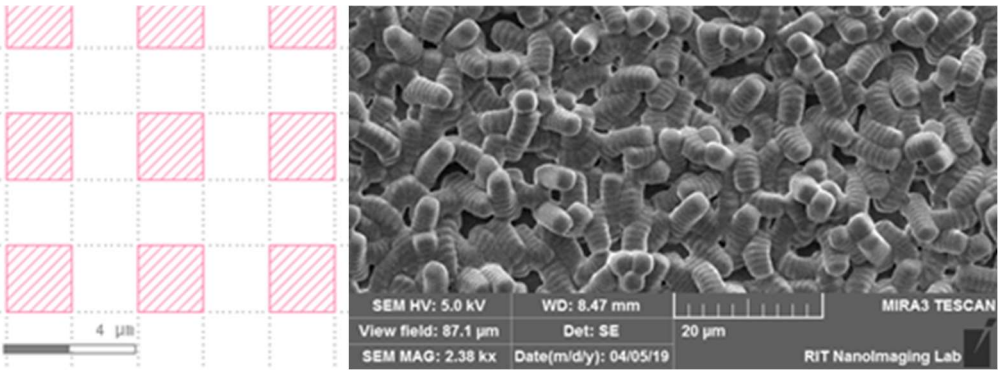

Figure 20 - 2µm free-standing pillars. Designed pattern (left), SEM image of sample PDMS-R6 (right)

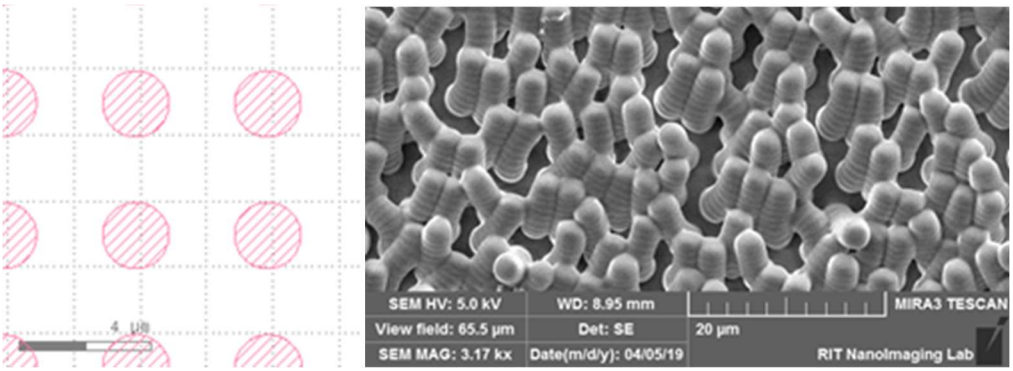

Figure 21 - 2µm diameter free-standing pillars. Designed pattern (left), SEM image of sample PDMS-R7 (right)

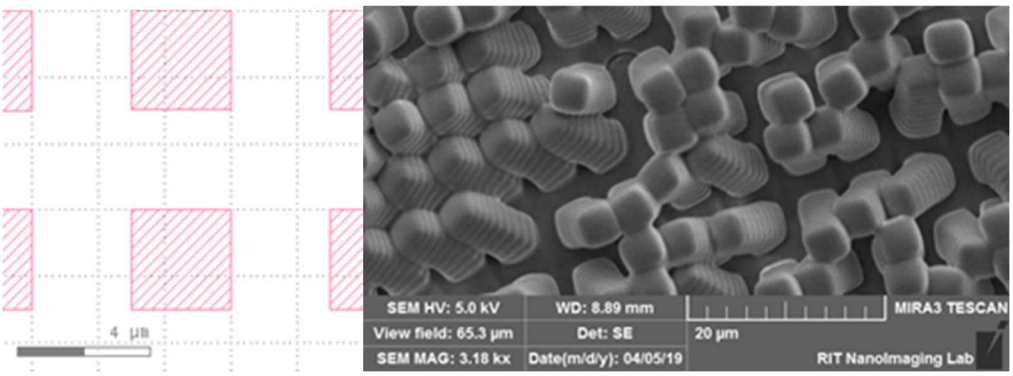

Figure 22 - 3µm free-standing pillars. Designed pattern (left), SEM image of sample PDMS-R8 (right)

All of the free-standing pillar patterns (samples PDMS-R4 – R8) resulted in replicas more akin to shag carpet than tall pillars, as shown by Figures 18-22. Despite this, high contact angles were measured (described below). Similarly to our 1µm checkerboard pattern, the square features of the 1µm and 2µm patterns resolved somewhat rounded instead, as we were again working near the minimum resolution of the lithography equipment. For the 2µm and 3µm patterns, this increased the contact angle of the surface, bringing them closest to the expected, Cassie-Baxter state contact angle.

Contact Angle Calculations and Measurements

Expected contact angles were calculated using the Cassie-Baxter equation,

$$\cos\theta_{CB} = f * \cos\theta_{Flat} - (1 - f)$$

Where f represents the fraction of the surface in contact with the liquid, and θ_{flat} represents the contact angle of the flat surface. Wenzel state contact angles [$\cos(\theta_W) = r*\cos(\theta_{flat})$, where r represents the roughness factor] were not calculated, as the tall aspect ratio of these patterns yields illogical results. These calculated Cassie-Baxter state contact angles allow us to predict surface performance using the

intended pattern diagrams. Unfortunately, as seen above, the actual etched and replicated patterns deviated from these planned arrays.

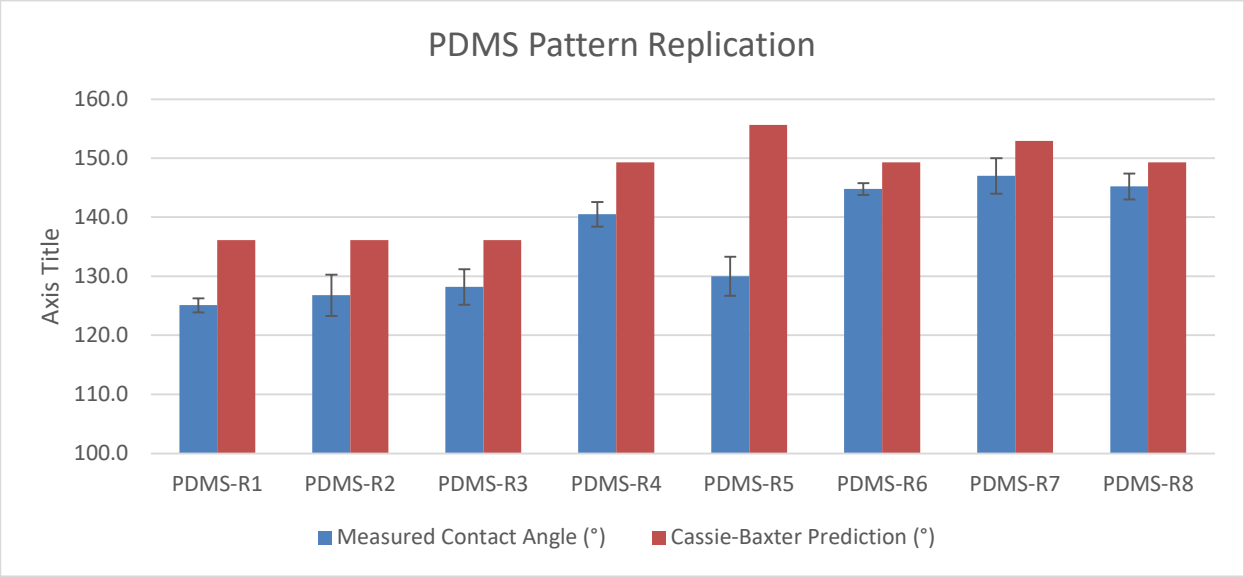

Figure 23 - Predicted and measured contact angles for PDMS replications of micron-scale patterns

As shown in Figure 23 and summarized in Table 7, checkerboard patterns (samples PDMS-R1 – R3) showed little variation in observed contact angle, slightly improving as feature size increased from 1μm to 3μm. This is likely due to the etched and replicated patterns more closely resembling the ideal, planned pattern as feature sizes increase. Free-standing pillar arrays (samples PDMS-R4 – R8) showed more variation in predicted and observed contact angles, with sample PDMS-R5 deviating most from the predicted contact angle. However, some of this deviation can be likely explained by the "shag carpet" appearance of the array, rather than the intended, ordered array.

Table 7 - Summary of predicted and measured contact angles for PDMS replications

Sample	**Contact Angle (°)**	**Standard Deviation (°)**	**Cassie-Baxter Predicted Contact Angle (°)**
PDMS-R1	125.1	1.2	136.1
PDMS-R2	126.8	3.5	136.1

PDMS-R3	128.2	3.0	136.1
PDMS-R4	140.5	2.1	149.3
PDMS-R5	130.0	3.3	155.6
PDMS-R6	144.8	1.0	149.3
PDMS-R7	147.0	3.0	152.9
PDMS-R8	145.2	2.2	149.3

6e. TIPS Process

Surfaces are produced from PMMA by first dissolving the polymer in a hot ethanol/water solution, then cooling the solution. The PMMA precipitates as the solution cools, forming microparticles which self-assemble to form a surface. The various fabrication parameters, including polymer molecular weight, polymer concentration, cooling temperature, and drying conditions all affected the surface topography and resulting contact angle. The surface topography was measured using a Hitachi S-900 High Resolution Near Field FE-SEM.

Effects of Molecular Weight

The majority of our work focused on one reference molecular weight PMMA and all testing was done using this molecular weight. However, additional work was performed using other molecular weights to better understand how these surfaces are formed, and to determine the sensitivity of the process regarding the properties of the starting material. With this reference PMMA material, we observed a contact angle of 132.7°±2.4° and particles with an average diameter of 2.21±0.64μm (average of 8 particles measured), as shown in Figure 24 and Figure 25. The surface was composed of packed microspheres with small, irregular voids throughout. These microparticles and voids provide the surface roughness needed to increase the contact angle from 66° to 133°.

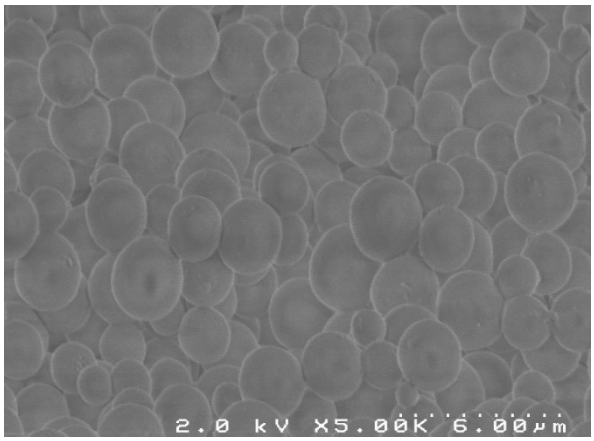

Figure 24 - SEM image of reference PMMA TIPS surfaces, showing spherical particles. Image distortion is due to charging effects on an electrically insulating surface.

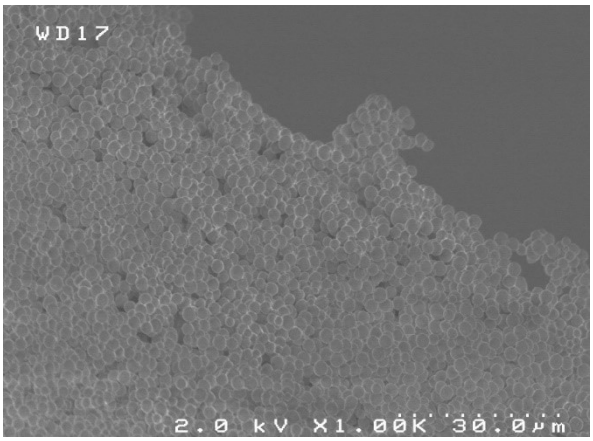

Figure 25 - SEM image of reference PMMA TIPS surface showing overall surface morphology

When the molecular weight is reduced to a lower molecular weight (~25% reduction in MW), we observed a similar water contact angle of 133.0°±4.0°, but a smaller average particle diameter of 1.16±0.38µm (average of 8 particles measured), as shown in Figure 26 and Figure 27. It was observed that some of these particles had grown to be oblong, and other particles appear to have grown together. When surfaces were produced at the same PMMA concentration as previous, reference surfaces, this lower molecular weight resulted in a visibly rough surface. However, when the concentration was reduced surfaces became thin and difficult to handle due to their fragility. The reduced particle size likely also reduced the size of interconnections between particles, reducing the overall durability of the surface.

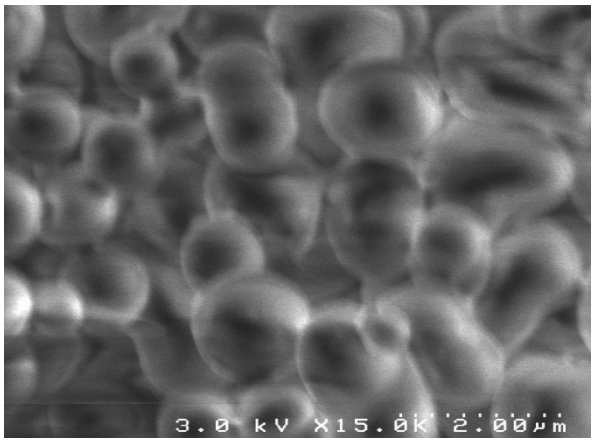

Figure 26 - SEM image of low MW PMMA TIPS surface showing oblong particles. Image distortion is due to charging effects on an electrically insulating surface.

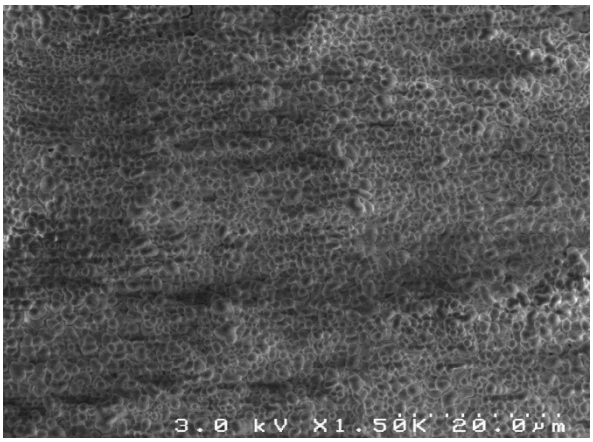

Figure 27 - SEM image of low MW PMMA TIPS surface showing overall surface morphology

When polymer molecular weight is increased (by ~20%), more drastic morphology changes were observed, as shown in Figure 28 and Figure 29. Individual particles were no longer observed and instead, particles appeared to grow together to form longer strings of small particles. The average particle diameter was lowest with this polymer weight, only 0.59±0.10μm. These morphology changes lead to the lowest observed contact angle, only 109.0°±4.8°, potentially due to the formation of more and larger gaps between (strings of) particles.

While the polymer would still readily form a colloidal solution when cooled to 20°C per our typical procedures, particles would not accumulate into a robust surface. This difficulty persisted despite being cooled further to -10°C in a freezer or being left for up to 4 days to precipitate. Even after this more extensive cooling and longer precipitation duration, a solid surface was not formed over the entire beaker floor, and the surface that was produced was very thin and fragile. Due to the combination of low contact angle and difficulty in surface formation, work using this polymer was stopped. This highlights the "sweet spot" of cooling rate, solubility and molecular weight for the manufacture of these samples, which suggests that others may not independently bear fruit when studying other polymers, given the large array of molecular weights available for commercial use.

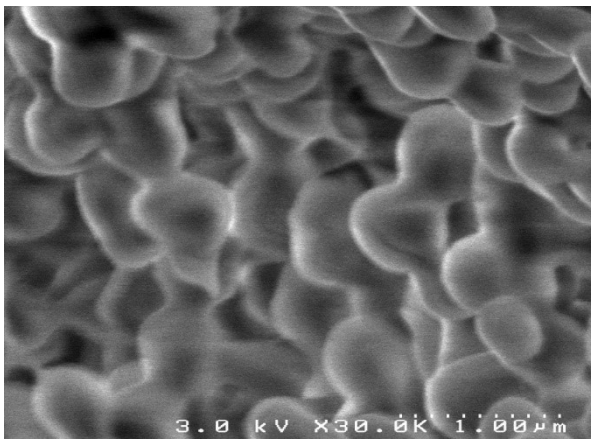

Figure 28 - SEM image of high MW PMMA TIPS surface showing particles grown together into strings. Image distortion is due to charging effects on an electrically insulating surface.

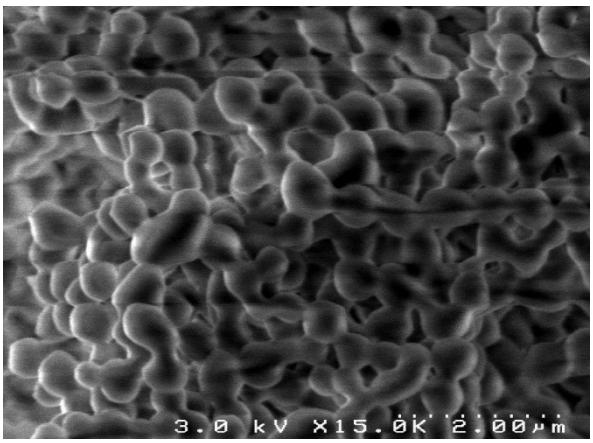

Figure 29 - SEM image of high MW PMMA TIPS surface showing surface morphology. Image distortion is due to charging effects on an electrically insulating surface.

Table 8 - Contact angle measurements and particle diameters for three molecular weights of PMMA

Sample	Contact Angle (°)	Standard Deviation (°)	Particle Diameter (µm)	Standard Deviation (µm)
Low MW	133.0	4.0	1.16	0.38
Reference PMMA	132.7	2.4	2.21	0.64
High MW	109.0	4.8	0.59	0.10

Effects of Polymer Concentration

Changes in the polymer concentration used to produce surfaces produce drastic changes to surface morphology. Work done by Yoneda *et al.*[51] produced tall polymer monoliths rather than smooth, flat surfaces using a very similar process. This work by Yoneda focused on polymer concentrations ranging from 0.04 – 0.08 g/mL, significantly different from our TIPS process. In an attempt to better understand how these surfaces form and how different manufacturing parameters affect the surface, a trial was conducted using this "literature polymer concentration" of 0.04 g/mL and compared to our TIPS surfaces. All other manufacturing steps were identical, but the resulting surface was drastically different as shown in Figure 30 and Figure 31. Rather than forming a smooth (on the order of 1mm thick), flat surface, a thick (several mm), rough, surface was formed. SEM images of samples produced at both polymer concentrations highlight the drastic changes. This again highlights the special "sweet spot" of manufacturing parameters for these highly hydrophobic structures.

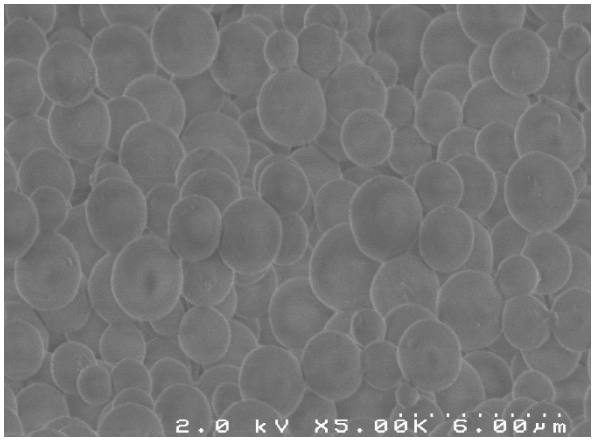

Figure 30 - PMMA TIPS surface

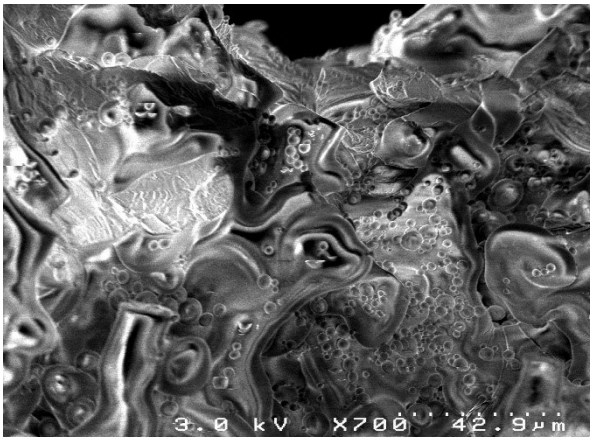

Figure 31 - PMMA surface at polymer concentration from literature[51]

When polymer concentration is too low, the resulting surface is thin, very fragile and often breaks into pieces during drying. When the polymer concentration is too high, the surface morphology transitions to forming a sponge-like porous structure with a visibly rough surface. However, at ideal concentrations, a smooth, flat, even surface of packed microspheres is formed.

This ideal concentration was initially found by conducting a series of tests at low concentrations, summarized below. This work was inspired by work done by Hoogenboom *et al*.,[14] which indicated that PS-PMMA copolymers can form a flat, porous structure through a thermally induced phase separation process. From other research and other attempts, we had learned/observed that porous structures can have hydrophobic properties. Our first attempts using the TIPS process were conducted at low concentrations of PMMA (only, not copolymer). A range of polymer concentrations were dissolved into 10 mL ethanol/water solvent solution. From these batches, 2 mL of each was dispensed into a small mold, placed into the refrigerator (at 10°C) and allowed to cool and precipitate for approximately 30 minutes. After precipitation, excess liquid was poured off and the resulting film was allowed to dry. Once fully dry, contact angle measurements were taken of each sample, summarized in Figure 32 and Table 9.

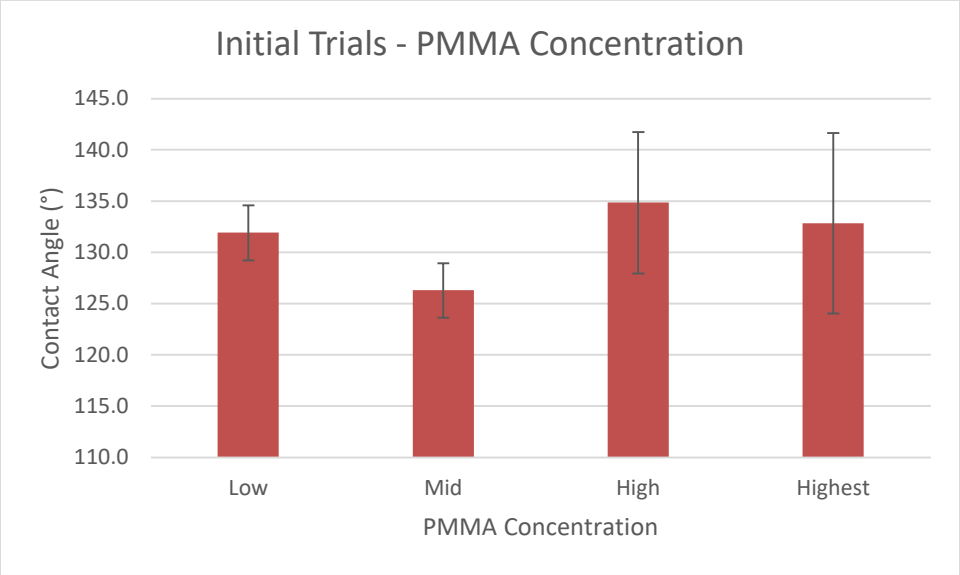

Figure 32 - Contact angle results from initial trials of producing PMMA surfaces through TIPS process

Despite its low contact angle measurements (relative to other concentrations), work was continued on the mid level polymer concentration due to the uniformity of its surface. The surface formed from low concentration PMMA was thin and did not cover the full surface of the mold. Surfaces formed at our high and highest PMMA concentrations were visibly rough and irregular, and it was assumed that this roughness would be detrimental to larger scale tests.

Table 9 – Summary of contact angle measurements for PMMA TIPS surfaces produced at various polymer concentrations

PMMA Concentration (g/mL)	Contact Angle (°)	Standard Deviation (°)
Low	131.9	2.7
Mid	126.3	2.7
High	134.9	6.9
Highest	132.8	8.8

Effects of Cooling/Precipitation Temperature

When surfaces were allowed to cool to room temperature (20°C) and precipitate (as opposed to the typical approach of cooling to 10°C), it was observed that the surface morphology was different on the underside of the surface when compared to the top. The upper surface remained consistent (visibly and in terms of contact angle) regardless of precipitation temperature (20°C room temperature or 10°C refrigerator), but the underside appeared clear and plastic-like when the solution is allowed to precipitate at room temperature. This irregularity in structure was not observed for surfaces cooled to and precipitated at 10°C, morphology for these surfaces appears identical on the top and on the underside of the surface, suggesting a consistent bulk structure throughout, again consistent with our manufacture of these samples at a sweet spot of fabrication parameters. It is unknown at this time if these changes in morphology are due to different cooling rates (slower cooling at room temperature, faster cooling when placed into the refrigerator), or if it is due to the polymer precipitating/settling at different temperatures. Additional, careful observation and study of the formation of these surfaces may explain more fully the cause of this change in morphology but was beyond the scope of this work.

Effects of Drying Conditions

One source of frustration when working with these surfaces is the tendency for free standing surfaces to warp during drying. This warping was not consistent, with some batches remaining relatively flat, and others warping severely. Additionally, this warping was not observed for surfaces produced in PS petri dishes, perhaps due to stronger adhesion between the PS and PMMA surfaces during the precipitation process. A method to reduce/eliminate this was found by adapting methods from Puppi *et al.*[52]. This group used computer aided wet spinning to form biomedical implants from PMMA, and also found that structures would shrink and warp during drying. However, by soaking as-produced, wet structures in either ethanol or water, this shrinking and warping could be reduced or eliminated.

We conducted two different trials using a method similar to that Puppi *et al.*[52] on our surfaces. The first attempt involved gently pouring water over a surface immediately after decanting the ethanol/water/polymer solution. Despite the gentle addition of water, the surface immediately became severely warped. We believed that the force of the water upon the surface was detrimental. On the second attempt, we allowed the surface to dry in air for 30 minutes before being removed from its beaker and transferred to a water bath. Likely due to its hydrophobic nature, the surface floated and needed to be weighed down by another beaker to remain submerged in the water bath. The surface was left in the water bath for 72 hours, and then was removed and allowed to dry. After this additional water soak step, no warping of the surface was observed, similar to the results observed by Puppi *et al*.. Contact angle measurements of this surface remained consistent with other measurements, indicating that no other detrimental changes to the surface morphology occurred due to this additional processing step.

Contact Angle Measurements and Abrasion/Wear Testing

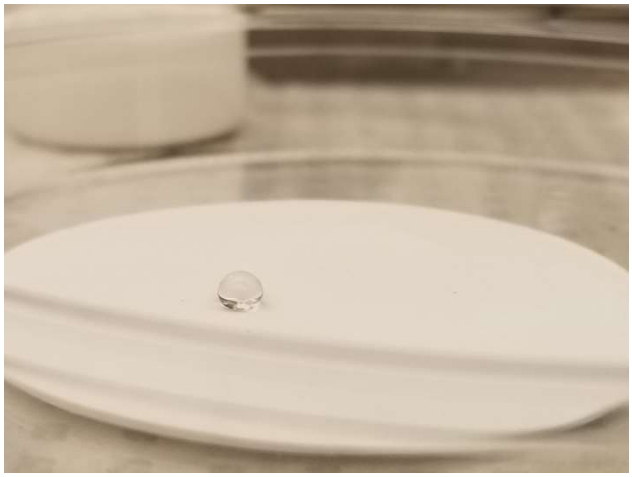

Figure 33 - Water droplet on PMMA surface produced through TIPS process (Mw=100k, 0.02 g/mL, 50mL solution precipitated in 150mL glass beaker overnight and dried in fume hood for 24 hours)

For each parameter set, abrasion testing was conducted on a total of six surface samples, to verify repeatability and the quality of data generated by our testing apparatus. It was hypothesized that the "packed spheres" structure of our hydrophobic surfaces would remain throughout the bulk, therefore being renewable with wear. If this hypothesis was confirmed, we would expect the surfaces to either maintain a consistent contact angle with wear or reach an equilibrium contact angle after some number of abrasion cycles (once any surface imperfections/irregularities have been worn away). To test this hypothesis, we performed a total of 20 abrasion cycles on each of the six surface samples, with contact angle measurements prior to testing and after 1, 5, 10, 15, and 20 abrasion cycles. Each of the six samples performed slightly differently in terms of contact angle, but with increase in abrasion the overall

trend is for no overall change, as shown in Figure 34 and summarized in Table 10. In other words, there is a consistent/stable average contact angle even as abrasion testing significantly wears down the surface. This indicates that the morphology of these surfaces remains consistent as the surface is worn down, and that we have developed a renewable surface. Optical microscope observations of fresh samples and abraded samples further supported this, with particle size, structure, and general morphology appearing to remain constant throughout the "bulk" of the tested surface. Fresh, as-produced samples showed some minor irregularities (i.e. hills and valleys), but these are quickly worn away, revealing a flat, consistent surface. Further testing using this, or a similar methodology could be used to estimate the useful lifetime of these surfaces, how long these surfaces would last before being completely worn away/worn through.

Table 10 - TIPS abrasion testing data

Sample:	Number of Abrasion Cycles					
	0	1	5	10	15	20
TIPS-A1	122.1° ± 3.7°	126.0° ± 3.4°	133.3° ± 8.6°	147.8° ± 2.0°	138.2° ± 3.2°	137.1° ± 5.8°
TIPS-A2	127.7° ± 2.7°	137.9° ± 9.5°	147.1° ± 1.6°	133.3° ± 5.5°	125.0° ± 0.6°	128.1° ± 4.4°
TIPS-A3	125.4° ± 7.1°	135.9° ± 7.1°	136.5° ± 2.7°	136.5° ± 2.7°	130.8° ± 2.8°	138.2° ± 2.8°
TIPS-A4	126.2° ± 9.4°	134.0° ± 3.6°	132.9° ± 1.1°	133.9° ± 1.1°	128.5° ± 5.2°	131.1° ± 1.6°
TIPS-A5	128.9° ± 3.3°	121.7° ± 2.5°	121.8° ± 2.0°	137.8° ± 5.3°	145.5° ± 5.4°	131.9° ± 5.3°
TIPS-A6	126.1° ± 4.3°	125.2° ± 3.0°	134.6° ± 3.6°	136.2° ± 6.1°	126.0° ± 2.7°	136.6° ± 7.6°
Overall:						
Average (°)	126.0	130.7	134.4	137.7	131.5	133.8
Standard Deviation (°)	4.7	7.9	8.2	6.1	6.8	5.7

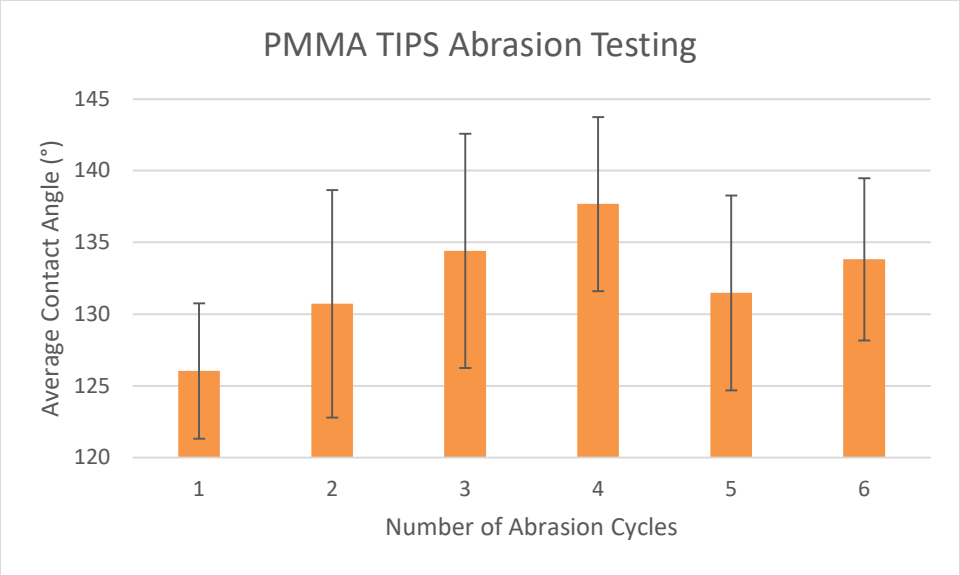

Figure 34 - Abrasion testing results for 6 PMMA TIPS surfaces (600 grit sandpaper, pressure applied by 250g mass)

6f. Replicating TIPS Process with Hansen Solubility Parameters

Following the success of the TIPS process in producing durable, hydrophobic surfaces, we attempted to replicate this process using additional, more robust polymers. PMMA, used exclusively in earlier trials, is less durable, less chemically resistant, and less thermally resistant than other, engineering polymers such as Ultem (a commercial poly(ether imide)). Hansen Solubility Parameters (HSP) theory offers a system or methodology for designing solvent systems with specific properties (Section 3e) and was used to design our experiments. Our goal was to first directly replicate the TIPS process, to design a solvent system which will only dissolve our target polymer when the solvent system is heated. This would allow us to again precipitate the polymer by cooling the polymer/solvent solution and produce surfaces with a TIPS-like morphology.

Our earlier work has shown that ethanol/water can be used to produce hydrophobic surfaces from PMMA (Section 6e) and we began work by first designing a second solvent system compatible with this same polymer. HSP values for PMMA and a wide range of solvents have been published by Dr. Hansen,[16] these values were used to design new solvent systems and predict their effectiveness. We selected miscible pairs of solvents whose HSP values lie outside of the target polymer sphere, as shown in Table 11 and Figure 35.

Table 11- HSP values for two example solvents and polymer PMMA

		δD	**δP**	**δH**	**R_a**
Polymer:	PMMA	18.6	10.5	5.1	11.0
Solvent 1:	Butyl Alcohol	16.0	5.7	15.8	
Solvent 2:	Water	15.5	16.0	42.3	

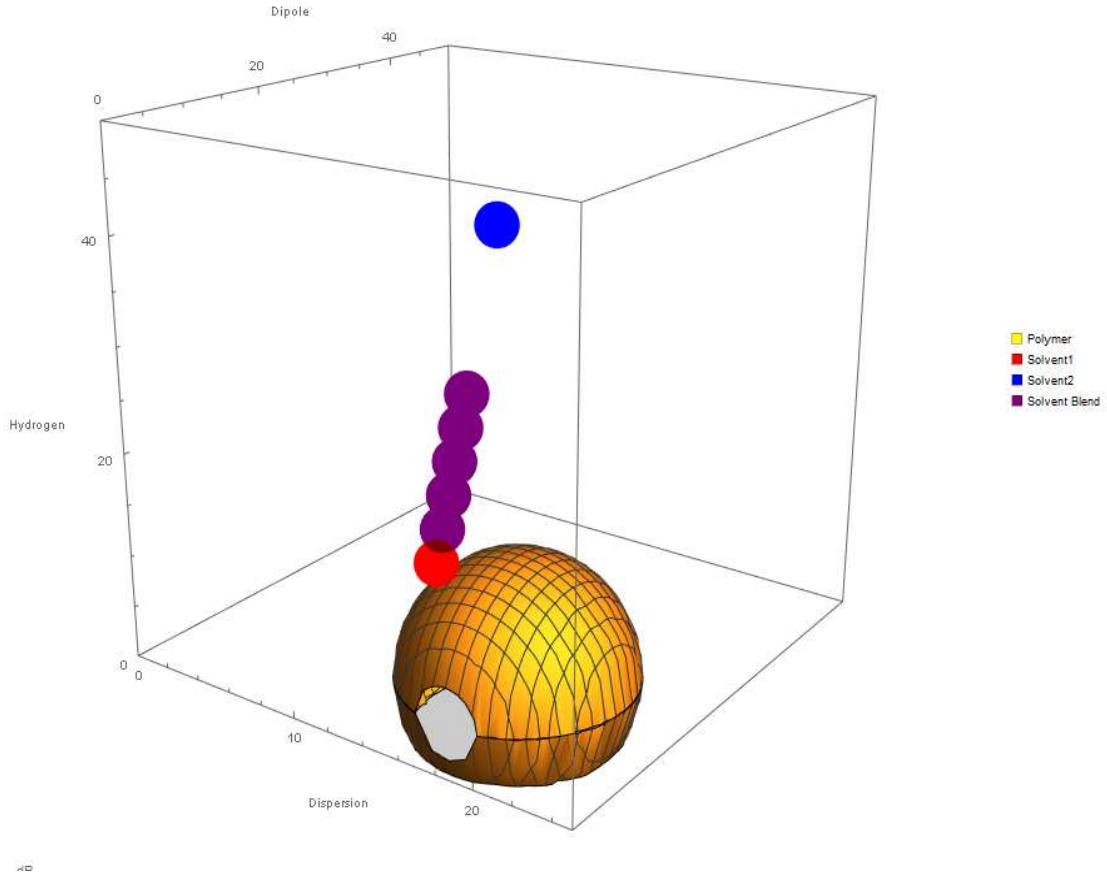

Figure 35 - PMMA, butyl alcohol, water, and blends of the two solvents in HSP space

By varying the proportions of these two solvents in the final solvent system, the system can be designed to have HSP values corresponding to any point on the line between them. Solvent ratios were selected to

test a range of radial distances between the solvent blends and polymer. We predicted that, as distances between the solvent and polymer decreased, solubility will increase. As all solvent systems (shown as purple points in Figure 35) lie outside the PMMA sphere, we did not expect the polymer to dissolve at room temperature.

Table 12 - HSP values and solubility results for butyl alcohol/water mixtures

	% Solvent 1	% Solvent 2	δD	δP	δH	R	Solubility - Room Temperature	Solubility - Heated
Blend1	50	50	15.8	10.9	29.1	24.6	None	Swelling
Blend2	60	40	15.8	9.8	26.4	22.0	None	Swelling
Blend3	70	30	15.9	8.8	23.8	19.5	None	Swelling
Blend4	80	20	15.9	7.8	21.1	17.1	None	Dissolved
Blend5	90	10	16.0	6.7	18.5	14.9	Minimal swelling	Dissolved
Blend6	100	0	16.0	5.7	15.8	12.8	None	Swelling

Similar experiments, using a range of solvents were conducted using PMMA and are summarized in Figure 36.

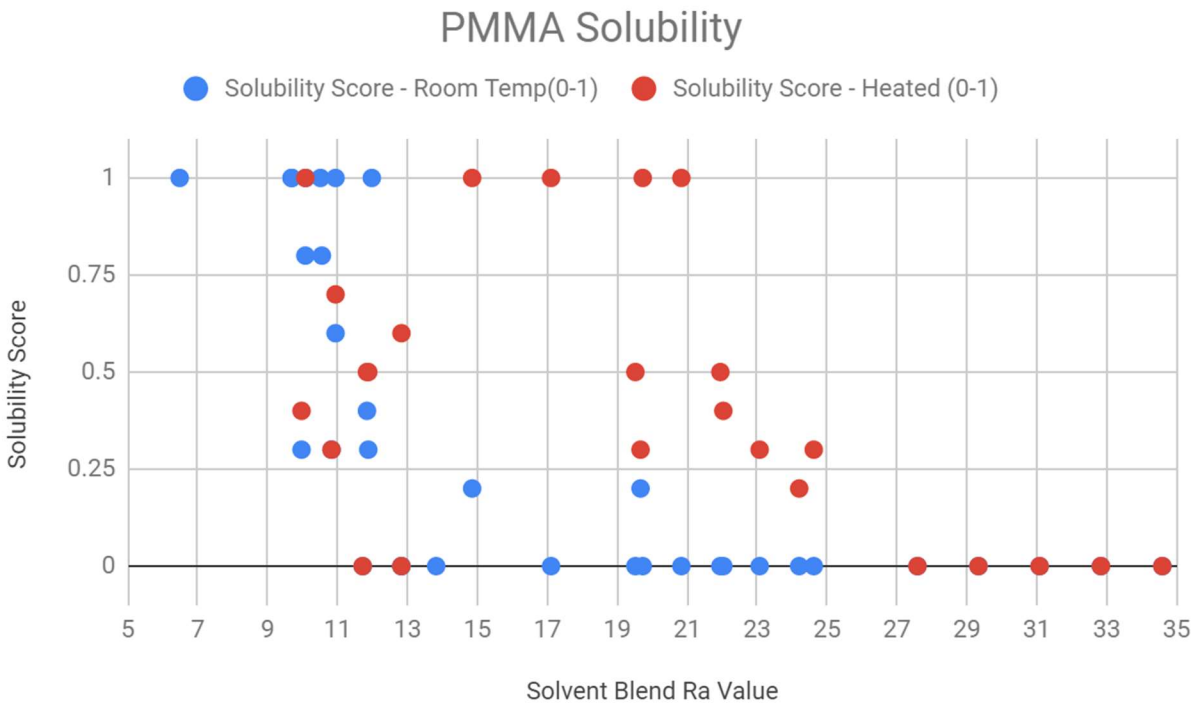

Figure 36 - PMMA solubility vs Solvent-Polymer radial distance. Pairs of vertically aligned blue and red dots correspond to the same solvent system before and after heating.

The first drop in solubility as R_a increases (blue points, at R_a=11-12) correlates well with the reported PMMA interaction radius of 11. Unfortunately, the second decrease in (heated solvent, red points) solubility is more broadened, lying between R_a=20-22, with several exceptions between R_a=10-13 (surrounding the reported polymer interaction radius). These initial results were encouraging, but also illustrate the overall challenge of this approach. Rather than a crisp and well-defined change in solubility at some given solvent-polymer radial distance, we found a much more gradual (and inconsistent) solubility change. Nevertheless, we began conducting similar trials with Ultem.

This work with Ultem encountered numerous challenges. Ultem HSP values (or poly(ether imides) in general) are not listed within Dr. Hansen's works[15,16] and no more recently published HSP values could be found for the specific grade of Ultem we selected (Ultem 1010). Thus, before HSP values could be used to determine ideal solvent systems, HSP values and interaction radius needed to be determined. This was accomplished by first testing for solubility in a range of single solvents, then observing their solubility over 48 hours at room temperature. Based on these initial results, several solvent blends were selected and also tested, summarized in

Table 13, below. Finally, the Solver add-in for Excel was used to find HSP values which minimized the radial distance of our experimentally found "good solvent" systems.

Table 13 – HSP values and Ultem solublity results

		δD	**δP**	**δH**	**R**	
Polymer:	Ultem	18.0	9.2	7.5	3.4	
Ultem Test 1		**δD**	**δP**	**δH**	**Ra**	
Solvent1	Pyridine	19	8.8	5.9	2.6	
Solvent2	Ethyl Acetate	15.8	5.3	7.2	5.9	
% Solvent 1	**% Solvent 2**	**δD**	**δP**	**δH**	**Ra**	**Result**
50	50	17.4	7.1	6.6	2.6	Slight swelling
60	40	17.7	7.4	6.4	2.2	Particles merged into puddle
70	30	18.0	7.8	6.3	1.9	Fully dissolved
80	20	18.4	8.1	6.2	1.9	Fully dissolved
90	10	18.7	8.5	6.0	2.1	Fully dissolved
Ultem Test 2		**δD**	**δP**	**δH**	**Ra**	
Solvent1	THF	16.8	5.7	8.0	4.3	
Solvent2	DMSO	18.4	16.4	10.2	7.7	
% Solvent 1	**% Solvent 2**	**δD**	**δP**	**δH**	**Ra**	**Result**
20	80	18.1	14.3	9.8	5.5	No change
30	70	17.9	13.2	9.5	4.5	No change
40	60	17.8	12.1	9.3	3.5	No change
50	50	17.6	11.1	9.1	2.6	Fully dissolved
65	35	17.4	9.4	8.8	1.8	Fully dissolved
80	20	17.1	7.8	8.4	2.4	Fully dissolved
90	10	17.0	6.8	8.2	3.3	Fully dissolved

Ultem Test 3		**δD**	**δP**	**δH**	**Ra**	
Solvent1	THF	16.8	5.7	8.0	4.3	
Solvent2	Acetonitrile	15.3	18.0	6.1	10.4	
% Solvent 1	**% Solvent 2**	**δD**	**δP**	**δH**	**R**	**Result**
100	0	16.8	5.7	8.0	4.3	Particles merged into puddle
90	10	16.7	6.9	7.8	3.5	Particles merged into puddle
80	20	16.5	8.2	7.6	3.2	Particles merged into puddle
60	40	16.2	10.6	7.2	3.9	Slight swelling
50	50	16.1	11.9	7.1	4.7	Slight swelling

When these "best guess" calculated Ultem HSP values were used in analysis of our previous results, we still found many inconsistencies. Several predicted "bad solvents" did have a significant effect on the polymer – in Ultem Test 3, 100% THF caused Ultem pellets to partially dissolve and merge into a single gel-like mass. Other predicted "good solvents" did not dissolve our polymer – in Ultem Test 1, a 1:1 blend of pyridine and ethyl acetate only caused slight swelling of Ultem, not the full dissolution that was predicted.

Many of our trials were successfully able to identify solvent systems which showed temperature dependent solubility with Ultem. Our polymer samples would be insoluble at room temperature, dissolve upon heating, and re-precipitate once cooled back to (below) room temperature. However, we were unable to replicate the one-pot sedimentation, self-assembly and solvent sintering hydrophobic surface formation that was observed with PMMA. Some solutions would precipitate into cloudy, colloidal suspensions (potentially due to polymer particles remaining too small to settle and form a surface), while others would form smooth "plastic like" surfaces with the same hydrophobic properties as uniform spin coated and flat Ultem surfaces (possibly precipitating too slowly to form discrete small particles).

6g. Sintered Microparticle Surfaces

The TIPS process consists of two general steps – forming microparticles from dissolved polymer, and fusing or sintering those particles into a cohesive, durable, hydrophobic surface. A literature search lead us to an emulsion process[18] which we adapted to produce <10µm Ultem particles. This was used to produce a broad distribution of particle sizes; vacuum filtration through progressively smaller pore size filters allowed us to test different size ranges and compare their effectiveness in terms of hydrophobicity.

These particles could then be sintered into similar hydrophobic surfaces by controlled exposure to solvent vapor.

The two particle size ranges selected were 5-10µm and 1-5µm. The most successful PMMA TIPS surfaces (in terms of durability and contact angles) were comprised of 2-3µm particles; the 1-5µm size range was selected to mimic these surfaces as closely as possible. We hypothesized that the smaller particles would form surfaces with higher contact angles, but lower surface durability while the larger particles would yield slightly lower contact angles and increased durability. As particle size decreases, surface roughness increases, leading to improved contact angles. However, interconnections between particles represent the "weak links" in the strength of the network of particles. As particles themselves get reduced in size, the number of these weak links per unit of area increases and the size of these links decreases, reducing the durability of the overall network of particles.

6g-1. PMMA Proof of Concept

Our first tests using this sintering process were designed to directly compare this new process to the self-assembly of the TIPS process by using similar materials and particles. By stirring the water/ethanol/dissolved PMMA TIPS solution as it cools, particles will still precipitate but will remain suspended. By using vacuum filtration, these suspended particles can be collected for initial sintering trials. Sintering was accomplished using a liquid good solvent/non-solvent blend.

When a 10% acetone/90% hexane solution was used, the PMMA powder did not form a cohesive surface, however using the same volume of 20% acetone/80% hexane, the PMMA powder did form a hydrophobic surface. When the acetone concentration was further increased to 30% and 35%, the dissolution process had progressed too far. While a solid surface was formed, it did not show the same hydrophobic properties as seen in earlier trials, indicating that the desired surface morphology had been lost. Final experiments to narrow down the ideal solvent concentration were conducted using 15% and 25% acetone solutions. Using a 15% Acetone solution resulted in a solid surface which crumbled easily upon handling, while 25% acetone produced results very similar to the 30% trial, suggesting a narrow "sweet spot" of acetone concentration of 15-20% v/v. Overall, the 15% and 20% acetone solutions appeared to produce the best results, yielding contact angles of 118.5° ± 2.0 (15% v/v acetone) and 124.2° ± 8.1° (20% v/v acetone), as summarized in Table 14, below.

To confirm the hydrophobic properties and to test the durability of these surfaces, abrasion testing was performed, and contact angle was measured (Figure 37, below). Using the same abrasion testing procedure as used on the TIPS surfaces from our previous work, 600 grit sandpaper, weighed down with a

250g mass, was pulled across our test surfaces. Contact angle measurements were taken after 1, 5, and 10 abrasion cycles and compared against initial measurements, taken before abrasion.

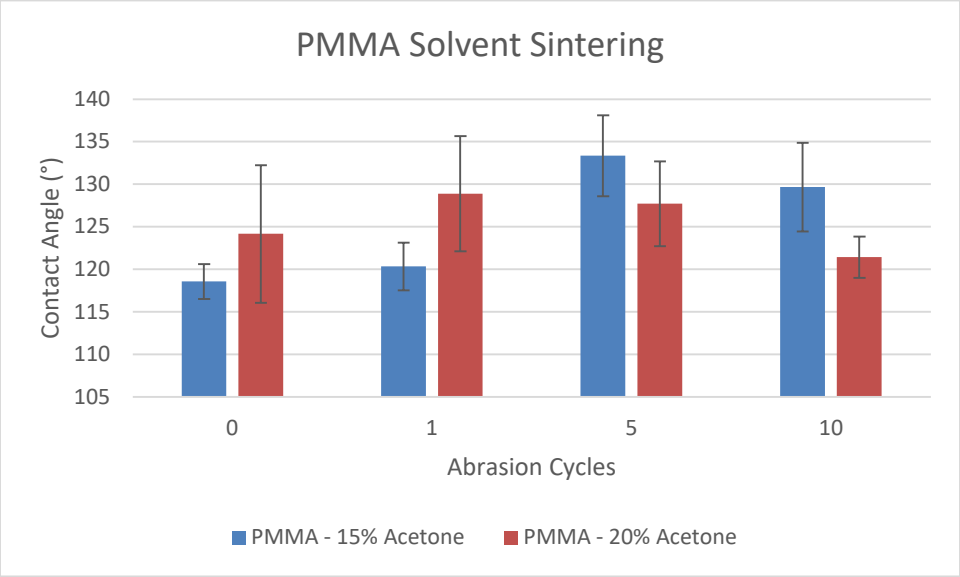

Figure 37 – Abrasion testing contact angle results for sintered PMMA surfaces

These abrasion test results follow a similar trend as our initial TIPS surfaces - slight improvements in contact angle after the first abrasion cycles, followed by a plateau/slight decrease. Subjectively, these surfaces appeared to wear more quickly than the TIPS surfaces, more material was removed during each abrasion cycle. However, this can likely be improved upon by applying pressure to the microparticle powder to further compact it and eliminate large voids before the application of the sintering solution, or by further optimizing the solvent concentration/immersion time.

Overall, this served as a successful proof of concept and our work moved on to using Ultem microparticles, produced in the lab using our Emulsion process. Surfaces produced from this, more resilient, polymer would make these surfaces viable for a wider range of applications.

Table 14 – Contact angle results for PMMA surfaces produced via solvent sintering

	15% Acetone / 85% Hexane		20% Acetone / 80% Hexane	
Number of Abrasions	Contact Angle (°)	Standard Deviation (°)	Contact Angle (°)	Standard Deviation (°)
0	118.6	2..0	124.2	8.1
1	120.3	2.8	128.9	6.8
5	133.4	4.8	127.7	5.0
10	129.7	5.2	121.4	2.4

6g-2. Single Emulsion/Solvent Evaporation Process

One effective method for producing polymer microparticles is through a single emulsion and solvent evaporation process.[18] In this process, polymer dissolved in an organic solvent is added to water and an emulsifier. These two liquids form an emulsion when stirred and the emulsified polymer micelles form solid microparticles as the organic solvent evaporates during stirring. While it had been shown that this process is compatible with a range of polymers,[18] published work focused on different polymers than we were interested in. Our first goal was therefore to determine the relationship between particle size and our two primary experimental variables – dissolved polymer concentration and stirring speed.

The first set of data collected examined particle diameter vs dissolved Ultem concentration. A consistent stirring speed of 1000 RPM was selected based on Dr. Sharma's results[18] where 1000 RPM stirring yielded particles with an average size of 900nm.[18] We then performed tests at a range of dissolved polymer concentrations. This range of concentrations both effects the viscosity of the solution and the total possible yield of microparticles. At low concentrations, very large batches (using large quantities of solvents) would need to be performed before sufficient quantities of microparticles to produce testable surfaces could be collected. However, at high concentrations, the high viscosity of the solution would

necessitate very high stirring speeds to break each droplet into sufficiently small microparticles, requiring additional equipment beyond what was available in our lab.

These experiments allowed us to produce a calibration curve (Figure 38, below) and predict the resulting average particle size based on the concentration of Ultem used.

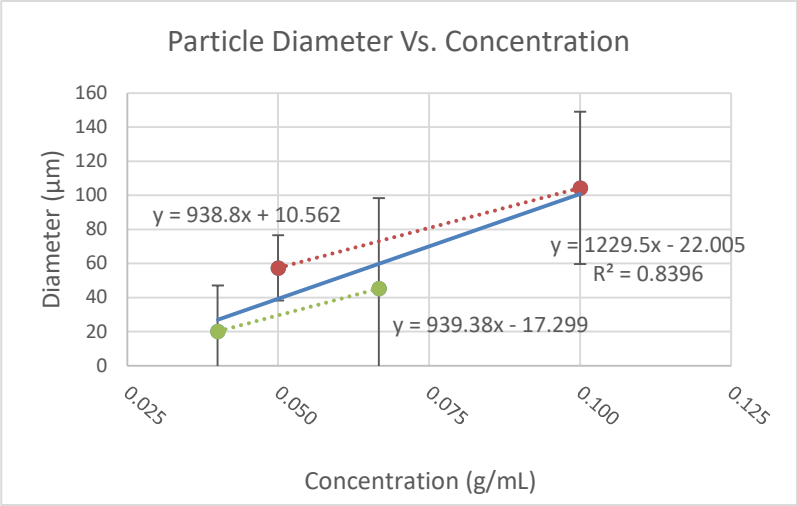

Figure 38 - Calibration curve - particle diameter vs dissolved Ultem concentration at fixed stirring speed of 1000 RPM. Note - two separate curves from two different hot plates.

These experiments had been run in parallel, with two different concentrations being used simultaneously on two different hotplates, each set to stir at 1000 RPM. When these samples were imaged and analyzed, it was readily apparent that the two hotplates used were not consistent in speed. When data from each hotplate was used to plot separate curves, the two lines (dotted red and green for the two hotplates) show near identical slopes. While exact measurements of stir speed or calibration were not performed, this still illustrates how sensitive these experiments can be to slight variations in experimental parameters. Once this was discovered, all future work was performed using one hotplate for consistency of data.

This data also illustrates the linear relationship between polymer concentration and resulting particle diameter, which offered us a simple means to control particle size and design experiments to specifically produce a given particle size. However, to produce our desired 1-5µm and 5-10µm diameter microparticles, an extremely low polymer concentration would be required (30mg/mL), severely limiting the scale of microparticles produced per (time consuming) experimental run.

Our second set of calibration curve experiments examined the relationship between particle size and stir speed, at a fixed concentration of 1g Ultem/20mL chloroform. This concentration represented, to us, the best compromise of high yield and low viscosity and the most likely candidate to produce the <10µm

particles we were most interested in. Our original set of experiments included trials performed at 400 and 600 RPM in addition to the ones shown in Figure 39, below. While trials ran at >800 RPM would readily form a homogeneous emulsion, at lower stir speeds a thin skin of Ultem would form on the surface of the mixture, suggesting that the desired homogeneous emulsion was not forming.

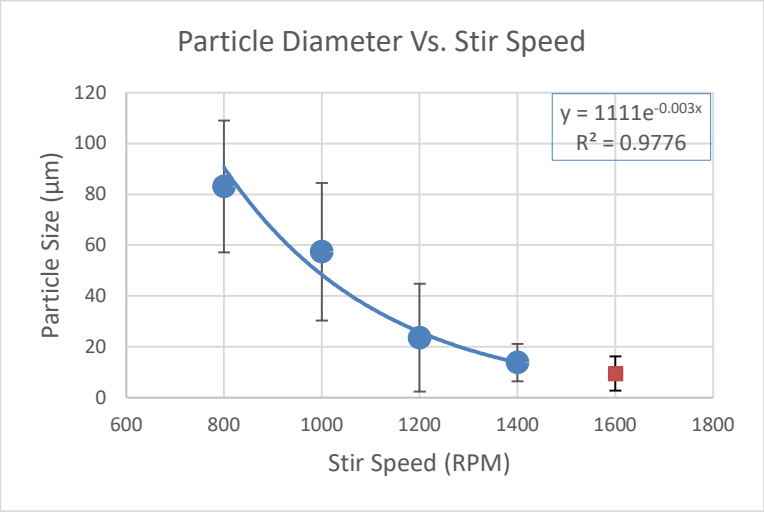

Figure 39 -- Calibration curve - particle diameter vs stir speed at fixed dissolved Ultem concentration of 1g Ultem/20mL chloroform.

These calibration curves only represent initial data but were sufficient to move forward with our work. Additional replication studies could improve these curves and verify their accuracy. Additionally, analysis was performed on a small sample from each produced batch of microparticles; we assume that the sample imaged is a representative sample of the whole batch and that particle size does not impact adhesion to the SEM sample holder. One side effect of using image analysis to measure particle sizes is SEM magnification/captured image resolution and algorithm requirements impose a "minimum recognizable particle size" and may skew reported distributions by incorrectly omitting small particles in each analyzed image.

After this calibration curve was completed, we moved on to examine if changing the batch size of this emulsion process would have an effect on particle size. To accomplish this, a second batch of particles was created using an Ultem concentration of 1g Ultem/20mL chloroform, stirred at 1200 RPM. During our original run, volumes used were 25mL Ultem/chloroform solution combined with 25mL PVA/water solution. For this "scaled up" run, these volumes were doubled to 50mL + 50mL, but all other experimental parameters were held constant. We found that at initial, small scales, produced microparticles were measured to have an average diameter of 24.0µm and a standard deviation of 7.4µm.

When scaled up, the produced microparticles were measured to have an average diameter of 21.4µm and a standard deviation of 9.0µm. From this extremely preliminary data, we concluded that this change in batch size did not have a significant impact on final particle size. However, this result is still preliminary and additional replication studies need to be done to better characterize particle sizes resulting from this emulsion process.

During production of high-RPM stir speed samples, the magnetic stir bar would often become unbalanced and cease stirring. The lack of stirring then led to recombination of still-liquid Ultem droplets within the emulsion and an erroneous increase in particle size. This issue was most common at smaller batch sizes (25mL PVA/water + 25mL Ultem/chloroform in 150mL beakers) and was much less common when batch sizes were increased to 50mL+50mL in 250mL beakers and using larger stir bars.

Given these challenges with high speed emulsions, we investigated alternative methods. We hypothesized that a bath- or probe- sonicator would produce an as-effective or more-effective emulsion, without the challenges posed by magnetic stir bars. Trials were performed which attempted to use a bath sonicator to produce the necessary emulsion. However, this did not impart enough energy to the solution and the two phases simply separated. We still hypothesize that a probe sonicator could be used to produce a much finer emulsion than our current methods, resulting in significantly smaller micro- or even nano- particles. This option was not pursued due to health concerns about capturing the evaporating chloroform solvent, but this could be managed with a different lab setup than we had access to.

The primary disadvantage of this process was the broad size distributions of particle sizes produced. As we were interested in particle sizes less than 10µm, this necessitated filtration before the particles could be effectively used to produce hydrophobic surfaces.

Our work has shown that this emulsion process is compatible with Ultem. We also performed successful proof-of-concept trials using polysulfone/chloroform. In the literature, Dr. Sharma's group has shown that this process is also compatible with PLGA 50:50 (poly(lactic-co-glycolic acid)), PLGA 75:25, and PLA (polylactide).[18] This versatility strongly suggests that this process can be easily adapted to a wide variety of polymers based on specific application requirements.

6g-3. Microparticle Filtration/Size Segregation

We were primarily interested in testing surfaces composed of 5-10µm and 1-5µm particles. Due to the broad size distribution of microparticles produced by the emulsion process, the particles required separation/sorting by size before they could be used to manufacture surfaces. In contrast to the success of the emulsion process, using multi-step vacuum filtration to separate these microparticles by size is a

process that still requires significant refinement. The two most significant issues caused by this filtration process are i) poor size segregation and ii) introduced contamination.

Poor size segregation was the most pressing issue to be corrected, as this was the primary reason for competing this step in our overall procedures. During planning, this appeared to be a simple process – the emulsion would be vacuum filtered through progressively finer filters, and we would collect microparticles within desired size ranges. However, in practice, this sharp size cutoff was not observed, as illustrated by the large particles in Figure 40.

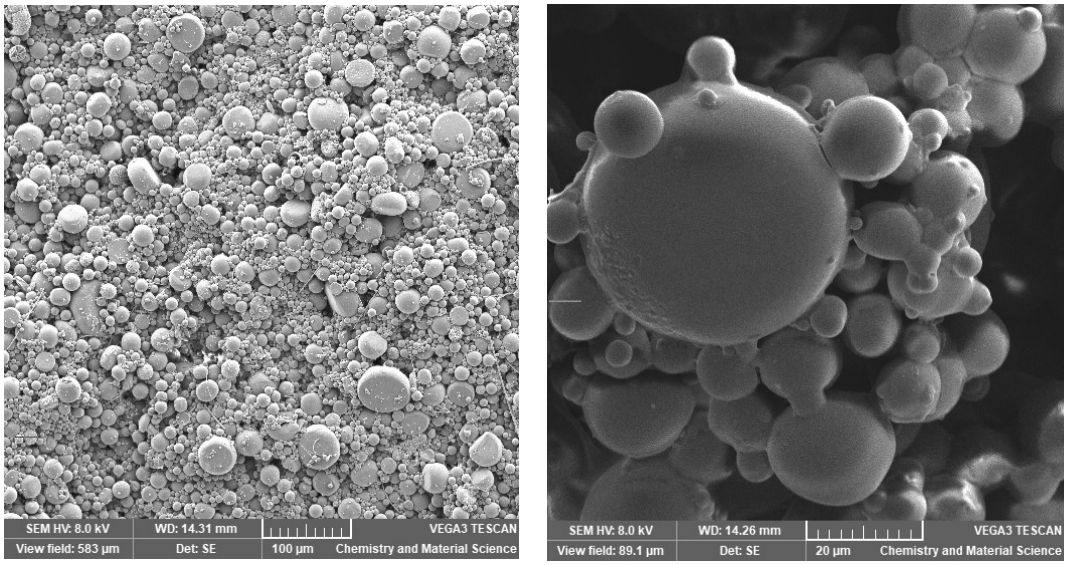

Figure 40 - Particles with expected sizes of 1-5µm (left - 100µm scale bar) and 5-10µm (right - 20µm scale bar)

Poor separation could have several causes. The number of microparticles filtered per filter paper could have been too high, leading to overpacking of the filter. As the number of particles collected on the surface of the filter paper increases, they begin to form an ever-thicker layer that all subsequent particles must pass through. This layer can act as another filter itself, trapping smaller-than-expected particles which would otherwise have passed through the filter paper. Cross-contamination from re-used glassware and filtration cups was also possible. The use of a strong vacuum pump may have led to additional compression of the filter paper during filtration, leading to a contraction of the filter pores, and retention of smaller than expected particles.

This final explanation is believed to be the primary cause of (or at least a significant factor in) the poor size separation observed. Over the first several minutes of each new filtration, the filter flow rate was observed to slow to a near stop as vacuum pressure builds within the collection flask. If pressure is equalized in this flask, and filtration resumed, the filter flow rate follows the same pattern of slowing to a

near stop. When the vacuum pump was replaced with a lower pressure aspirator-style pump, this decrease in flow rate was significantly reduced, although separation remained imperfect.

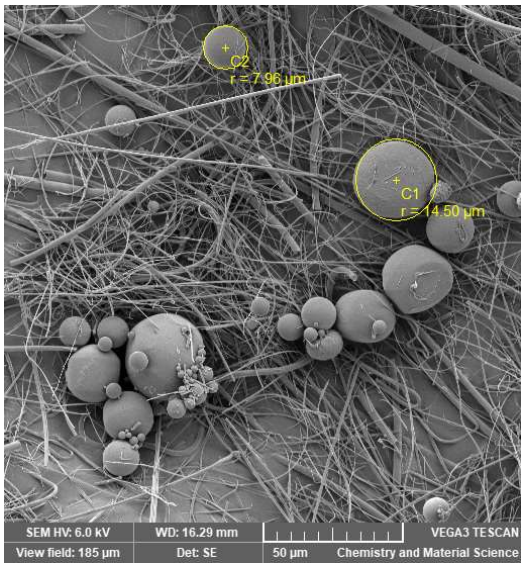

Figure 41 - Collected Ultem microparticles with filter fiber contamination.

One additional side effect of using filters to capture our microparticles is the introduction of contamination in the form of filter fibers when the microparticles are removed from the filter. If a mechanical process is used to scrape captured particles from the filter, or a liquid washing process is used while the filter paper is still wet, filter fibers can also be collected, contaminating the particles, as shown in Figure 41. When the filters and captured particles are first fully dried, particles can be collected by immersing the filter in boiling water and gently agitating. This is the method used during our trials, as it leads to the most complete removal of particles from the filter and minimizes filter fiber contamination.

All of these filtrations and washing steps only further illustrate the need for a better solution for size separation of produced microparticles. Future work could investigate the use of a dry sieving process or perforated/fritted filters to improve both the quality of separation and simplicity of the overall process. Alternatively, microfluidic systems may be used to produce much more narrow size distributions of particles, eliminating the need for complex multi-stage filtration processes (Section 7c, below).

6g-4. Solvent Sintering

When we first began work decomposing the TIPS process into its separate steps, we used a liquid sintering process to form microparticles into hydrophobic surfaces. The sintering solution used was a miscible blend of a good solvent and a non-solvent; when particles were submerged in this solution, the good solvent would begin to slowly dissolve the outer edges of each particle, forming interconnections.

However, we looked ahead to the production of a real-world coatings using a mold, we began to doubt if this would be the correct approach. With this liquid sintering process, the eventual evaporation of the good solvent stops the sintering process. As this evaporation occurs and the solvent level steadily decreases, portions of the prototype inside its mold would be exposed to the sintering solution for longer or shorter durations, leading to uneven sintering and performance. We hypothesized that the same sintering process could be induced by solvent vapor and began planning proof-of-concept trials.

The goal of our first set of experiments was to confirm that solvent vapor sintering would indeed form the same types of interconnections between particles as the TIPS process and liquid sintering. By performing sintering at a range of durations, we could also use the data gathered to determine the ideal sintering time to maximize hydrophobicity and surface durability.

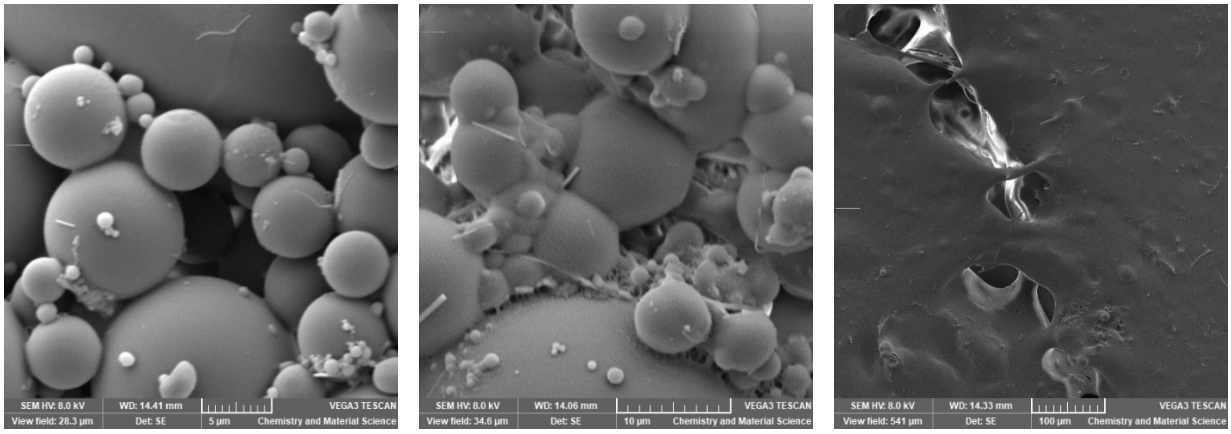

Figure 42 - 1-5µm particles sintered with chloroform vapor for 30 minutes (left), 75 minutes (center), and 2 hours (right)

Images taken from samples sintered for 30 minutes, 75 minutes, and 2 hours (Figure 42, above) clearly show how interconnections between discrete particles steadily grow, with a textured layer of loose particles slowly dissolving into a smooth, featureless blob. While these results are similar to those from the TIPS process, the (still) wide particle size distribution prevents optimal packing, and thus limits overall surface strength and robustness. Nonetheless, these were very promising initial results – this new process works to sinter loose particle into a cohesive surface and, by careful selection of sintering times, surfaces can be designed to have increased surface roughness (at the cost of smaller interconnections and decreased strength) or increased strength (at the cost of decreased surface roughness).

During this solvent sintering process, the polymer microparticles take on solvent as solvent molecules begin to disentangle polymer chains from the bulk. This absorption of solvent and disentanglement causes the microparticles to swell in size, pressing adjacent particles together and allowing polymer chains from one particle to become entangled with chains in other particles. It is in this swollen state that

the interconnections, which give the overall surface its strength, initially form. When the sintering process is ended and the solvent vapor atmosphere is removed, these swollen particles reduce back to their original size, (over) stressing their newly formed interconnections, and leading to fault line-like cracks in the surface, as shown in Figure 43. Similar to the warping initially observed with TIPS surfaces, we hypothesize by controlling and slowing the final evaporation of retained solvent from the final surface, particles and their interconnections would have more time to solidify, strengthen, and more evenly distribute these stresses and that this cracking could be reduced or eliminated.

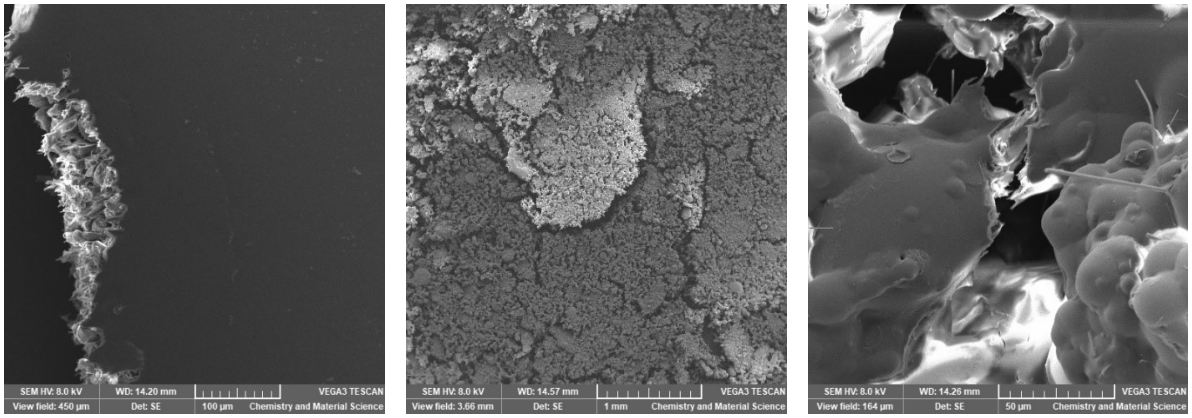

Figure 43 - Ultem microparticle surfaces cracking during/after sintering. Left - 5-10µ particles sintered for 2 hours. Center - 1-5µm particles sintered for 90 minutes. Right - 1-5µm particles sintered for 105 minutes.

Our primary metric to evaluate the performance of these sintered surfaces was again through contact angle measurements. Initial measurements were taken from samples produced from both 5-10µm and 1-5µm particles that had been sintered for durations ranging from 30 minutes to 150 minutes. These results are summarized in Table 15.

Table 15 - Contact angle results from initial testing of sintered Ultem surfaces

	1-5µm Particles		**5-10µm Particles**	
Sinter Duration	**Contact Angle (°)**	**StdDev (°)**	**Contact Angle (°)**	**StdDev (°)**
30 min	absorbs instantly		absorbs within a few seconds	
45 min	absorbs instantly		absorbs within a few seconds	
60 min	absorbs within a few seconds		110.1	6.9
75 min	absorbs within a few seconds		absorbs within a few seconds	
90 min	absorbs within a few seconds		74.4	6.6
105 min	86.1	11.8	(not tested)	
120 min	82.9	1.2	90.1	8.4
150 min	(not tested)		81.3	4.3

A total of 14 samples were produced and tested, one sample for each particle size/duration combination. From this, very initial, data results are inconclusive. For over half (8 total) of the samples, the surfaces absorb the test water droplet before the goniometer optics can be correctly focused and a measurement taken. Of the 6 samples that were able to be measured, 5 samples showed statistically significant improvement in contact angle. This suggests that this sintering process does effectively produce hydrophobic surfaces, and that TIPS-like morphologies result in increased hydrophobicity regardless of the materials used. However, the large number of samples which absorbed the droplet show that additional refinement of this process is needed.

The increase in contact angle shown by these Ultem surfaces is much smaller than the increase shown in PMMA through the TIPS process. With these (preliminary) Ultem surfaces, contact angle increased from 70.0° (flat) to 110.1° (sintered surface). However, with PMMA, we observed an increase from 66.1° (flat) to 132.7° (sintered surface). We believe that this discrepancy is due to the wide particle size distribution used to manufacture the Ultem sintered surfaces. Once this distribution can be reduced, surface morphology will likely more closely match that of PMMA TIPS surfaces, and we expect surface hydrophobicity to increase.

We initially hypothesized that larger microparticles would require a longer sintering duration in order to form equally robust surfaces as those produced from smaller particles, but this was not observed. It was thought that a larger particle volume would require a similarly larger volume of solvent to induce the same degree of dissolution as with smaller particles and would thus require a longer sintering duration. If anything, our initial results suggest that larger particles actually require a shorter sintering duration. However, further testing of additional surfaces must be performed before this hypothesis can be accurately examined.

The high contact angles shown by these sintered particle surfaces (Table 15) suggest that additional study and abrasion testing are warranted in future work. However, work needs to be done to improve the uniformity of particle sizes used to produce these surfaces before additional testing is performed, as described in Section 7c, below.

7. Future Work

7a. TIPS

Further work on the TIPS process could examine further the effects of molecular weight, polydispersity, and stereochemical configuration on final surface morphology and hydrophobicity. Additional BET (Brunauer-Emmett-Teller) measurements could be used to determine and quantify the porosity of these materials, potentially identifying applications for these surfaces. Finally, the inclusion of some form of dye concentration gradient could act as a "wear indicator" – as the surface is worn away, the surface dye concentration would change and could be monitored as an indicator of remaining surface thickness/lifespan.

7b. Tuned Pattern Surfaces

Continued work using tuned patterns could be used to produce features with varying heights/aspect ratios to better understand how the "three-dimensionality" of these patterns impacts their performance. Patterns could be developed to test for a "critical feature size" responsible for a transition between Wenzel and Cassie-Baxter wetting states. These tests could be repeated using a range of different replication polymers, quantifying the effects of chemistry vs morphology. Replication can be repeated using a more rigid polymer, allowing for testing of more accurately replicated surfaces. Patterns could also be designed to facilitate fluid handling on lab-on-a-chip devices – tuned hydrophilic and hydrophobic areas could encourage fluid flow in desired directions.

7c. Emulsion Process Surfaces

In their work, "Preparation of Monodisperse Biodegradable Polymer Microparticles Using a Microfluidic Flow-Focusing Device for Controlled Drug Delivery," Xu, *et al*. demonstrate that microfluidic devices can be used to produce monodisperse polymer microparticles[53]. This process uses similar principles as our work present here, with droplets of dissolved polymer forming in a PVA/water carrier liquid. Resulting particle size can be controlled by varying the flow rate through the device. This type of process could be used to build upon and improve upon the work presented here. By producing monodisperse particles, the need for complicated filtration processes would be eliminated. Additionally, uniformity in particle sizes used would likely lead to better particle packing within sintered surfaces, resulting in improved surface durability.

By testing surfaces produced from particles with a range of sizes (i.e. 1µm, 2µm, 3µm, 4µm, …), trends in contact angles could identify if there exists a "critical feature size" transition between Wenzel and

Cassie-Baxter wetting states. Identification of this transition point could guide future surface development and allow for better simultaneous optimization of both surface roughness/hydrophobicity and durability.

By testing identical surfaces produced from different polymers, additional work could also quantify the effects of strict surface morphology versus polymer chemical structure. One underlying hypothesis of our work has been that, through careful design of surface morphology, inherently hydrophilic materials can be engineered to be hydrophobic. Through careful production and sintering of surfaces produced with identical morphologies but from different materials, this hypothesis could finally be accurately tested.

8. Conclusions

Our initial experiments with PVC and blended PS/PMMA surfaces (Sections 4b and 4c, above) allowed us to explore different methods and approaches to producing hydrophobic polymer surfaces. While not perfect solutions themselves, these initial insights into hydrophobicity and hydrophobic surface morphologies led to the development of our TIPS process (Section 4g, above).

The newly developed Thermally Induced Phase Separation (TIPS) Process has been shown to effectively produce durable hydrophobic surfaces from PMMA. These surfaces are produced from a very narrow "sweet spot" of experimental parameters using green chemistry techniques. These surfaces were demonstrated to retain their hydrophobic properties after abrasion due to their unique 3-dimensional structure and interconnected particle morphology.

While these TIPS surfaces show a dramatic improvement in water contact angle and improved durability of these hydrophobic properties (Section 6e), the poor thermal and chemical resilience of PMMA limits the range of applications for these surfaces. Work then progressed to adapting this process (only demonstrated using PMMA) to be compatible with a range of polymers (Sections 4f and 4g). This culminated in the development of an emulsion and solvent sintering process.

Through this work with polymer emulsions and solvent sintering (Section 4g), we have successfully deconstructed the previously discovered TIPS process into its component steps and have demonstrated, through proof-of-concept trials, that this process can be applied to a variety of different polymers to produce hydrophobic surfaces. While several steps of this new process still require optimization, we have identified other work within the literature which could be adapted to overcome currently identified challenges (Section 7c, above).

While less appropriate for large-scale production, our work with lithographically produced, tuned pattern surfaces (Section 4d) has allowed us to gain a better understanding of ideal feature sizes and the impact of minor changes in size, spacing, geometry, etc., on a surface's hydrophobic properties. By studying these idealized surfaces alongside chemically produced surfaces, we were able to design future experiments based on prior successes. Several interesting research questions, however, were left unanswered and offer opportunities for future work (Section 7b, above).

9. Works Cited

(1) Cassie, A. B. D.; Baxter, S. Wettability of Porous Surfaces. *Trans. Faraday Soc.* **1944**, *40*, 546. https://doi.org/10.1039/tf9444000546.

(2) Wenzel, R. N. RESISTANCE OF SOLID SURFACES TO WETTING BY WATER. *Ind. Eng. Chem.* **1936**, *28* (8), 988–994. https://doi.org/10.1021/ie50320a024.

(3) Simpson, J. T.; Hunter, S. R.; Aytug, T. Superhydrophobic Materials and Coatings: A Review. *Rep. Prog. Phys.* **2015**, *78* (8), 086501. https://doi.org/10.1088/0034-4885/78/8/086501.

(4) Barbier, C.; Jenner, E.; D'Urso, B. Drag Reduction With Superhydrophobic Riblets. In *Volume 8: Mechanics of Solids, Structures and Fluids*; American Society of Mechanical Engineers: Houston, Texas, USA, 2012; pp 199–205. https://doi.org/10.1115/IMECE2012-86029.

(5) Wu, X.; Chen, Z. A Mechanically Robust Transparent Coating for Anti-Icing and Self-Cleaning Applications. *J. Mater. Chem. A* **2018**, *6* (33), 16043–16052. https://doi.org/10.1039/C8TA05692G.

(6) Lin, Y.; Chen, H.; Wang, G.; Liu, A. Recent Progress in Preparation and Anti-Icing Applications of Superhydrophobic Coatings. *Coatings* **2018**, *8* (6), 208. https://doi.org/10.3390/coatings8060208.

(7) Ding, Y.; Xu, W.; Yu, Y.; Hou, H.; Zhu, Z. One-Step Preparation of Highly Hydrophobic and Oleophilic Melamine Sponges via Metal-Ion-Induced Wettability Transition. *ACS Appl. Mater. Interfaces* **2018**, *10* (7), 6652–6660. https://doi.org/10.1021/acsami.7b13626.

(8) Crick, C. R.; Ozkan, F. T.; Parkin, I. P. Fabrication of Optimized Oil–Water Separation Devices through the Targeted Treatment of Silica Meshes. *Science and Technology of Advanced Materials* **2015**, *16* (5), 055006. https://doi.org/10.1088/1468-6996/16/5/055006.

(9) Malavasi, I.; Bernagozzi, I.; Antonini, C.; Marengo, M. Assessing Durability of Superhydrophobic Surfaces. *Surface Innovations* **2015**, *3* (1), 49–60. https://doi.org/10.1680/si.14.00001.

(10) Mortazavi, V.; Khonsari, M. M. On the Degradation of Superhydrophobic Surfaces: A Review. *Wear* **2017**, *372–373*, 145–157. https://doi.org/10.1016/j.wear.2016.11.009.

(11) Callister, W. D.; Rethwisch, D. G. *Materials Science and Engineering: An Introduction*; 2018.

(12) Brown, J. L.; Nair, L. S.; Laurencin, C. T. Solvent/Non-solvent Sintering: A Novel Route to Create Porous Microsphere Scaffolds for Tissue Regeneration. *J. Biomed. Mater. Res.* **2008**, *86B* (2), 396–406. https://doi.org/10.1002/jbm.b.31033.

(13) Miller-Chou, B. A.; Koenig, J. L. A Review of Polymer Dissolution. *Progress in Polymer Science* **2003**, *28* (8), 1223–1270. https://doi.org/10.1016/S0079-6700(03)00045-5.

(14) Hoogenboom, R.; Becer, C. R.; Guerrero-Sanchez, C.; Hoeppener, S.; Schubert, U. S. Solubility and Thermoresponsiveness of PMMA in Alcohol-Water Solvent Mixtures. *Aust. J. Chem.* **2010**, *63* (8), 1173. https://doi.org/10.1071/CH10083.

(15) Hansen, C. M. *The Three Dimensional Solubility Parameter and Solvent Diffusion Coefficient: Their Importance in Surface Coating Formalation*; Danish Technical Press, 1967.

(16) Hansen, C. M. *Hansen Solubility Parameters: A User's Handbook*, 2nd ed.; CRC Press: Boca Raton, 2007.

(17) Rosca, I. D.; Watari, F.; Uo, M. Microparticle Formation and Its Mechanism in Single and Double Emulsion Solvent Evaporation. *Journal of Controlled Release* **2004**, *99* (2), 271–280. https://doi.org/10.1016/j.jconrel.2004.07.007.

(18) Sharma, N.; Madan, P.; Lin, S. Effect of Process and Formulation Variables on the Preparation of Parenteral Paclitaxel-Loaded Biodegradable Polymeric Nanoparticles: A Co-Surfactant Study. *Asian Journal of Pharmaceutical Sciences* **2016**, *11* (3), 404–416. https://doi.org/10.1016/j.ajps.2015.09.004.

(19) Milionis, A.; S., I.; Fragouli, D.; Brandi, F.; Athanassiou, A. Combination of Lithography and Coating Methods for Surface Wetting Control. In *Updates in Advanced Lithography*; Hosaka, S., Ed.; InTech, 2013. https://doi.org/10.5772/56173.

(20) Lee, H.; Koh, D.; Xu, L.; Row, S.; Andreadis, S.; Oh, K. A Simple Method for Fabrication of Microstructures Using a PDMS Stamp. *Micromachines* **2016**, *7* (10), 173. https://doi.org/10.3390/mi7100173.
(21) Kalin, M.; Polajnar, M. The Wetting of Steel, DLC Coatings, Ceramics and Polymers with Oils and Water: The Importance and Correlations of Surface Energy, Surface Tension, Contact Angle and Spreading. *Applied Surface Science* **2014**, *293*, 97–108. https://doi.org/10.1016/j.apsusc.2013.12.109.
(22) *Conceptual Models of Flow and Transport in the Fractured Vadose Zone: Papers Presented at a Workshop Held in March 1999*; U.S. National Committee for Rock Mechanics, National Research Council, National Research Council, Eds.; National Acad. Press: Washington, DC, 2001.
(23) Young, T. III. An Essay on the Cohesion of Fluids. *Phil. Trans. R. Soc. Lon* **1805**, *95*, 65–87. https://doi.org/10.1098/rstl.1805.0005.
(24) Ali, H. M.; Qasim, M. A.; Malik, S.; Murtaza, G. Techniques for the Fabrication of Super-Hydrophobic Surfaces and Their Heat Transfer Applications. In *Heat Transfer - Models, Methods and Applications*; Volkov, K., Ed.; InTech, 2018. https://doi.org/10.5772/intechopen.72820.
(25) Kim, S. H. Fabrication of Superhydrophobic Surfaces. *Journal of Adhesion Science and Technology* **2008**, *22* (3–4), 235–250. https://doi.org/10.1163/156856108X305156.
(26) Herrmann, C. F.; DelRio, F. W.; Bright, V. M.; George, S. M. Conformal Hydrophobic Coatings Prepared Using Atomic Layer Deposition Seed Layers and Non-Chlorinated Hydrophobic Precursors. *J. Micromech. Microeng.* **2005**, *15* (5), 984–992. https://doi.org/10.1088/0960-1317/15/5/013.
(27) Berkowski, K. L.; Plunkett, K. N.; Yu, Q.; Moore, J. S. Introduction to Photolithography: Preparation of Microscale Polymer Silhouettes. *J. Chem. Educ.* **2005**, *82* (9), 1365. https://doi.org/10.1021/ed082p1365.
(28) Chang, B.; Leussink, P.; Jensen, F.; Hübner, J.; Jansen, H. DREM: Infinite Etch Selectivity and Optimized Scallop Size Distribution with Conventional Photoresists in an Adapted Multiplexed Bosch DRIE Process. *Microelectronic Engineering* **2018**, *191*, 77–83. https://doi.org/10.1016/j.mee.2018.01.034.
(29) Wu, B.; Kumar, A.; Pamarthy, S. High Aspect Ratio Silicon Etch: A Review. *Journal of Applied Physics* **2010**, *108* (5), 051101. https://doi.org/10.1063/1.3474652.
(30) Saenz, C. Procedure for Silanization of SU-8/Silicon Master. Microfluidics/Microfabrication Facility, Harvard Medical School October 17, 2015.
(31) Keßler, S.; Schmid, F.; Drese, K. Modeling Size Controlled Nanoparticle Precipitation with the Co-Solvency Method by Spinodal Decomposition. *Soft Matter* **2016**, *12* (34), 7231–7240. https://doi.org/10.1039/C6SM01198E.
(32) Janting, J.; Pedersen, J. K. M.; Inglev, R.; Woyessa, G.; Nielsen, K.; Bang, O. Effects of Solvent Etching on PMMA Microstructured Optical Fiber Bragg Grating. *J. Lightwave Technol.* **2019**, *37* (18), 4469–4479. https://doi.org/10.1109/JLT.2019.2902244.
(33) Fernández-Piérola, I.; Horta, A. Cosolvents of PMMA. *Makromol. Chem.* **1981**, *182* (6), 1705–1714. https://doi.org/10.1002/macp.1981.021820611.
(34) Li, L.; Li, R.; Li, M.; Rong, Z.; Fang, T. Theoretical Selection of Solvent for Production of Electrospun PMMA Fibers with Wrinkled Surfaces. *RSC Adv.* **2014**, *4* (53), 27914. https://doi.org/10.1039/c4ra03657c.
(35) Seitz, M.; Podbielski, P.; Collison, C. Smart Materials For Improved Fuser Membranes. August 2019.
(36) Painter, P. C.; Coleman, M. M. *Fundamentals of Polymer Science: An Introductory Text*, 2nd ed.; Technomic Pub. Co: Lancaster, Pa, 1997.
(37) Chu, X.; Chung, W.; Schmidt, L. D. Sintering of Sol-Gel-Prepared Submicrometer Particles Studied by Transmission Electron Microscopy. *J American Ceramic Society* **1993**, *76* (8), 2115–2118. https://doi.org/10.1111/j.1151-2916.1993.tb08344.x.

(38) Nukavarapu, S. P.; Kumbar, S. G.; Brown, J. L.; Krogman, N. R.; Weikel, A. L.; Hindenlang, M. D.; Nair, L. S.; Allcock, H. R.; Laurencin, C. T. Polyphosphazene/Nano-Hydroxyapatite Composite Microsphere Scaffolds for Bone Tissue Engineering. *Biomacromolecules* **2008**, *9* (7), 1818–1825. https://doi.org/10.1021/bm800031t.
(39) Wang, F. J.; Lei, S.; Ou, J. F.; Xue, M. S.; Li, W. Superhydrophobic Surfaces with Excellent Mechanical Durability and Easy Repairability. *Applied Surface Science* **2013**, *276*, 397–400. https://doi.org/10.1016/j.apsusc.2013.03.104.
(40) Chen, H.; Yuan, Z.; Zhang, J.; Liu, Y.; Li, K.; Zhao, D.; Li, S.; Shi, P.; Tang, J. Preparation, Characterization and Wettability of Porous Superhydrophobic Poly (Vinyl Chloride) Surface. *J Porous Mater* **2009**, *16* (4), 447–451. https://doi.org/10.1007/s10934-008-9217-8.
(41) Ma, Y.; Cao, X.; Feng, X.; Ma, Y.; Zou, H. Fabrication of Super-Hydrophobic Film from PMMA with Intrinsic Water Contact Angle below 90°. *Polymer* **2007**, *48* (26), 7455–7460. https://doi.org/10.1016/j.polymer.2007.10.038.
(42) Tian, X.; Verho, T.; Ras, R. H. A. Moving Superhydrophobic Surfaces toward Real-World Applications. *Science* **2016**, *352* (6282), 142–143. https://doi.org/10.1126/science.aaf2073.
(43) Verho, T.; Bower, C.; Andrew, P.; Franssila, S.; Ikkala, O.; Ras, R. H. A. Mechanically Durable Superhydrophobic Surfaces. *Adv. Mater.* **2011**, *23* (5), 673–678. https://doi.org/10.1002/adma.201003129.
(44) Basu, B. B. J.; Paranthaman, A. K. A Simple Method for the Preparation of Superhydrophobic PVDF–HMFS Hybrid Composite Coatings. *Applied Surface Science* **2009**, *255* (8), 4479–4483. https://doi.org/10.1016/j.apsusc.2008.11.065.
(45) Jung, Y. C.; Bhushan, B. Mechanically Durable Carbon Nanotube−Composite Hierarchical Structures with Superhydrophobicity, Self-Cleaning, and Low-Drag. *ACS Nano* **2009**, *3* (12), 4155–4163. https://doi.org/10.1021/nn901509r.
(46) Collison, C. J.; Rothberg, L. J.; Treemaneekarn, V.; Li, Y. Conformational Effects on the Photophysics of Conjugated Polymers: A Two Species Model for MEH−PPV Spectroscopy and Dynamics. *Macromolecules* **2001**, *34* (7), 2346–2352. https://doi.org/10.1021/ma001354d.
(47) Con, C.; Cui, B. Effect of Mold Treatment by Solvent on PDMS Molding into Nanoholes. *Nanoscale Res Lett* **2013**, *8* (1), 394. https://doi.org/10.1186/1556-276X-8-394.
(48) Dann, J. R. Forces Involved in the Adhesive Process. *Journal of Colloid and Interface Science* **1970**, *32* (2), 321–331. https://doi.org/10.1016/0021-9797(70)90055-X.
(49) Hammami, M. A.; Croissant, J. G.; Francis, L.; Alsaiari, S. K.; Anjum, D. H.; Ghaffour, N.; Khashab, N. M. Engineering Hydrophobic Organosilica Nanoparticle-Doped Nanofibers for Enhanced and Fouling Resistant Membrane Distillation. *ACS Appl. Mater. Interfaces* **2017**, *9* (2), 1737–1745. https://doi.org/10.1021/acsami.6b11167.
(50) Chuah, Y. J.; Koh, Y. T.; Lim, K.; Menon, N. V.; Wu, Y.; Kang, Y. Simple Surface Engineering of Polydimethylsiloxane with Polydopamine for Stabilized Mesenchymal Stem Cell Adhesion and Multipotency. *Sci Rep* **2016**, *5* (1), 18162. https://doi.org/10.1038/srep18162.
(51) Yoneda, S.; Han, W.; Hasegawa, U.; Uyama, H. Facile Fabrication of Poly(Methyl Methacrylate) Monolith via Thermally Induced Phase Separation by Utilizing Unique Cosolvency. *Polymer* **2014**, *55* (15), 3212–3216. https://doi.org/10.1016/j.polymer.2014.05.031.
(52) Puppi, D.; Morelli, A.; Bello, F.; Valentini, S.; Chiellini, F. Additive Manufacturing of Poly(Methyl Methacrylate) Biomedical Implants with Dual-Scale Porosity. *Macromolecular Materials and Engineering* **2018**, *303* (9), 1800247. https://doi.org/10.1002/mame.201800247.
(53) Xu, Q.; Hashimoto, M.; Dang, T. T.; Hoare, T.; Kohane, D. S.; Whitesides, G. M.; Langer, R.; Anderson, D. G. Preparation of Monodisperse Biodegradable Polymer Microparticles Using a Microfluidic Flow-Focusing Device for Controlled Drug Delivery. *Small* **2009**, *5* (13), 1575–1581. https://doi.org/10.1002/smll.200801855.